

Constraining the Hubble constant to a precision of about 1% using multi-band dark standard siren detections

Liang-Gui Zhu,^{1,2} Ling-Hua Xie,¹ Yi-Ming Hu,^{1,2,*} Shuai Liu,^{1,2,†} En-Kun Li,^{1,2,‡}
Nicola R. Napolitano,¹ Bai-Tian Tang,¹ Jian-dong Zhang,^{1,2,§} and Jianwei Mei^{1,2}

¹*School of Physics and Astronomy, Sun Yat-sen University (Zhuhai Campus), Zhuhai 519082, P.R. China*

²*MOE Key Laboratory of TianQin Mission, TianQin Research Center for Gravitational Physics, Frontiers Science Center for TianQin, CNSA Research Center for Gravitational Waves, Sun Yat-sen University (Zhuhai Campus), Zhuhai 519082, P.R. China*

(Dated: May 16, 2022)

Gravitational wave signals from stellar-mass black hole binary inspiral can be used as standard sirens to perform cosmological inference. Such inspiral covers a wide range of frequency bands, ranging from the millihertz band to high frequency band, so that both space-borne and ground-based gravitational wave detectors can observe. In this work, we perform a comprehensive study on the ability of constraining the Hubble constant with the dark standard sirens, or gravitational wave events without the electromagnetic counterparts. In order to obtain the redshift information, we weight the galaxies within the localization error box according to the multiple band photometric information, and use them as a proxy for the binary black hole redshift. We find that, TianQin is expected to constrain the Hubble constant to a precision of about 30% through 10 gravitational wave events detections; in the most optimistic case, the Hubble constant can be constrained to a precision of $< 10\%$, if TianQin I+II is assumed. The multi-detector network of TianQin and LISA is capable of constraining the Hubble constant to within 5% precision in the optimistic case. It is worth highlighting that the multi-band network of TianQin and Einstein Telescope can constrain the Hubble constant to a precision close to 1%. We conclude that it is feasible to infer the Hubble constant with photo-z, for which we also demonstrate the self-consistency through the P–P plot. On the other hand, high quality spectroscopic redshift could play an critical role in improving the estimation precision.

* huyiming@mail.sysu.edu.cn

† liushuai5@mail.sysu.edu.cn

‡ lienk@mail.sysu.edu.cn

§ zhangjd9@mail.sysu.edu.cn

I. INTRODUCTION

The gravitational wave (GW) observations of compact binary coalescences can be used as standard sirens, thanks to the fact that the intrinsic GW strength can be deduced from the phase evolution [1]. Combined with the redshift information, which can be obtained through the electro-magnetic (EM) observations, such standard sirens can be used to determine cosmological parameters.

The Hubble constant can be determined by the late Universe measurements, represented by the type Ia supernova (SN Ia) observations, and by the early Universe measurements, represented by the cosmic microwave background (CMB) anisotropies observations. However, there is a significant inconsistency between these two measurement values, and the inconsistency has grown over 4σ [2–9], this discrepancy, also known as the ‘Hubble tension’, has become a hot topic. Although the luminosity distance measurement is usually accompanied with large statistical errors, they are still regarded as an important probe, as the GW observation can provide a direct measurement of the luminosity distance that is independent of the cosmic distance scale ladder. Therefore, the standard sirens possess a potential of clarifying the Hubble tension [10–12].

The direct detection of the GW signals from compact binary coalescences by LIGO and Virgo [13–26] opened an era of GW astronomy. Among different types of GW signals, the binary neutron stars (BNSs) and neutron star-black hole binaries (NSBHs) mergers are ideal standard sirens since they have the potential to be detected through both the GW and the EM channels. The current ground-based GW detectors, including KAGRA [27] and LIGO-India [28], is expected to detect dozens of GW events of BNSs and NSBHs during the operation, and a few percent precision of the Hubble constant is expected to be reached from the GW cosmology [10, 29–31]. The first multi-messenger observations of a BNS merger event GW170817 [18, 32–34], provided the first standard siren measurement of the Hubble constant, $H_0 = 70.0^{+12.0}_{-8.0}$ km/s/Mpc [35] (also see [36–38]).

The stellar-mass binary black hole (SBBH) mergers are expected to be dark in the EM channel [cf. 39, 40], therefore, the cosmological constraint from SBBHs can only be derived through the “dark standard siren” [1, 41]. In this scenario, the redshift information is provided by matching the GW source sky localization and the galaxies catalogues. It is expected that the current ground-based GW detectors can still effectively constrain the Hubble constant by the SBBHs GW events [10, 36, 41–51], and indeed constraint of the Hubble constant has already been obtained with the observation of GW170814 and GW190814, provided a measurement precision of about 57% [41–44].

The future ground-based GW detectors, such as Einstein Telescope (ET) [52–54] and Cosmic Explorer (CE) [55, 56], will be much more sensitive, and can detect GW events at higher redshift. This enable the potential of not only measuring the Hubble constant, but also constraining other cosmological parameters [57–71]. On the other hand, space-borne GW detectors that operate in the millihertz band, like TianQin [72] and LISA [73], can observe GW signals at cosmological distances, including massive black hole binaries (MBHBs) [74–76], extreme mass ratio inspirals (EMRIs) [77–79], and SBBHs [80, 81]. The space-borne GW detectors are expected to have excellent sky localization ability, which also allows them to constrain the Hubble constant as well as other cosmological parameters [82–94].

The SBBHs are very interesting GW sources, as their GW signals cover a wide frequency range from millihertz to kilohertz. This feature enables the GW signals of SBBHs to be detectable in multiple band [95, 96]. Space-borne GW detectors can observe the early inspiral signal while ground-based GW detectors can study the final merger. The observation of both low frequency and high frequency can be complimentary, with space-borne detectors can measure phase information more precisely [80, 81] and ground-based detectors are expected to accumulate higher signal-to-noise ratios (SNRs) [58], thus improving the overall parameter estimation precision of GW source [97–100], so that one can better extraction of physical/astronomical information [97, 101–105] and measurement of the expansion of the Universe [106].

In this work, we study the potential of constraining the Hubble constant with TianQin using the SBBH GW sources. Furthermore, the anticipated operation time of the various detectors allows simultaneous observation of a multi-detector network of TianQin [107, 108] and LISA [73], as well as a multi-band network of TianQin and ET [54]. We thus study how such networks can help to better constrain the Hubble constant.

We design the organization of this paper as follows. In Section II, we present the cosmological analytical framework and introduce the methods needed for the spatial localizations of GW sources and the weighting of candidate host galaxies. In Section III, we introduce the astrophysical background needed for the simulations and present the simulation method of observational data. In Section IV, we illustrate the constraint processes of the cosmological parameters and show the constraint results on the Hubble constant. In Section V, we discuss several key issues in the analyses and the simulations. In Section VI, we summarize our findings and discuss the needs of future research.

II. METHODOLOGY

Throughout the work, we adopt a spatially-flat Lambda cold dark matter (Λ CDM) cosmology. In the late Universe, the Hubble parameter, which describes the expansion rate of the scale factor, can be expressed as

$$H(z) = H_0 \sqrt{\Omega_M(1+z)^3 + \Omega_\Lambda}, \quad (1)$$

where $H_0 \equiv H(z=0)$ is the Hubble constant that describes the current expansion rate, and $\Omega_M, \Omega_\Lambda = 1 - \Omega_M$ are the fractional densities for total matter and dark energy with respect to the critical density $\rho_c = 3H_0^2/(8\pi G)$ (where G is Newton's gravitational constant), respectively. Such cosmology predicts that the luminosity distance D_L of a source with redshift z is

$$D_L = c(1+z) \int_0^z \frac{1}{H(z')} dz', \quad (2)$$

where c is speed of light in vacuum. Throughout this work, we use $H_0 = 67.8$ km/s/Mpc and $\Omega_M = 0.307$ [2] as the injected true values.

A. Standard siren and dark standard siren

The two polarizations of GW signal of an inspiralling binary with component masses m_1 and m_2 can be described as [109]

$$h_+(t) = \left(\frac{G\mathcal{M}_z}{c^2}\right)^{5/3} \left(\frac{\pi f(t)}{c}\right)^{2/3} \frac{2(1+\cos^2\iota)}{D_L} \cos(\Psi(t, \mathcal{M}_z, \eta)), \quad (3a)$$

$$h_\times(t) = \left(\frac{G\mathcal{M}_z}{c^2}\right)^{5/3} \left(\frac{\pi f(t)}{c}\right)^{2/3} \frac{4\cos\iota}{D_L} \sin(\Psi(t, \mathcal{M}_z, \eta)), \quad (3b)$$

where $\mathcal{M}_z = (1+z)\mathcal{M} = (1+z)(m_1 m_2)^{3/5}/(m_1 + m_2)^{1/5}$ is the redshifted chirp mass (with a perfect degeneracy between the redshift and the physical mass), $\eta = m_1 m_2/(m_1 + m_2)^2$ is the symmetric mass ratio, ι is the inclination angle of the binary orbital angular momentum with respect to line of sight, and $\Psi(t, \mathcal{M}_z, \eta)$ is the phase of the GW signal. Notice that the overall amplitude is only dependant on the redshifted chirp mass, the inclination, and luminosity distance. The mass parameter \mathcal{M}_z can be accurately inferred from the GW phase evolution, and the inclination angle can be determined through the amplitude ratio between different polarizations. Therefore, compact binary coalescences are referred to as standard siren, as it is possible to infer the luminosity distance D_L directly from the GW data.

In order to determine the cosmological parameters, one still needs the redshift information, which the GW data analysis can hardly provide. In the following, we list several methods that can be used to obtain the redshift information [110]:

- The EM counterpart. The coalescence of BNS and NSBH are usually accompanies with EM radiation like short Gamma ray bursts [34, 111, 112] or kilonovae [113–115]. In such cases, the redshift can be determined directly [30, 35, 37].
- The “dark standard siren”. Galaxies are clustered in small scales. Assuming the GW sources are linked with a host galaxy, one can obtain a statistical understanding of the redshift based on the galaxy information even without the EM counterpart [41, 42, 45, 47, 49, 84, 91, 92, 94].
- The neutron star mass distribution. EM observations deduced a relatively narrow distribution for masses of neutron stars in BNSs. This intrinsic distribution can be used to break the mass-redshift degeneracy [46, 59, 63, 116].
- The tidal deformation of the neutron stars. A compact object with finite size will undergo tidal deformation during the coalescence, leading to phase correction of the GW waveform. The degree of tidal deformation is determined by both the intrinsic mass and the equation of state of the neutron star, so the correcting phase can break the mass-redshift degeneracy [61, 62].
- The cross-correlation method. EM observations have mapped out the spatial distribution of the galaxies in redshift space, and GW detections can also map out the spatial distribution of the GW events in luminosity distance space, then the cross-correlation of spatial distributions between the galaxies and the GW sources can be used to extract redshift information [50, 117–120].

- Other methods. There are also efforts to use the mass distribution of SBBH population [48, 70], the intrinsic redshift probability distribution of compact binary mergers [121, 122], and high-order correction of the GW waveform phase due to cosmic acceleration [123–125], *etc.*, to break degeneracy and obtain redshift information.

In this work, we consider the dark standard siren scenario with SBBHs to constrain the Hubble constant H_0 .

B. Bayesian framework

We adopt a Bayesian analytical framework to infer the cosmological parameters from the dark standard siren data and the catalogues of survey galaxies [10, 35, 36, 90]. Consider a set of GW detection data composed of N GW events $\mathcal{D}_{\text{GW}} \equiv \{d_{\text{GW}}^1, d_{\text{GW}}^2, \dots, d_{\text{GW}}^i, \dots, d_{\text{GW}}^N\}$ as well as the corresponding EM observation data set $\mathcal{D}_{\text{EM}} \equiv \{d_{\text{EM}}^1, d_{\text{EM}}^2, \dots, d_{\text{EM}}^i, \dots, d_{\text{EM}}^N\}$, the posterior probability distribution of the cosmological parameter set $\vec{H} \equiv \{H_0, \Omega_M\}$ is given by

$$p(\vec{H}|\mathcal{D}_{\text{GW}}, \mathcal{D}_{\text{EM}}, I) = \frac{p_0(\vec{H}|I)p(\mathcal{D}_{\text{GW}}, \mathcal{D}_{\text{EM}}|\vec{H}, I)}{p(\mathcal{D}_{\text{GW}}, \mathcal{D}_{\text{EM}}|I)} = \frac{p_0(\vec{H}|I) \prod_i p(d_{\text{GW}}^i, d_{\text{EM}}^i|\vec{H}, I)}{p(\mathcal{D}_{\text{GW}}, \mathcal{D}_{\text{EM}}|I)}, \quad (4)$$

where $p_0(\vec{H}|I)$ is the prior probability distribution for \vec{H} , I indicates all the relevant background information. The normalisation factor $p(\mathcal{D}_{\text{GW}}, \mathcal{D}_{\text{EM}}|I)$ is also known as Bayes evidence, which is independent of \vec{H} . Therefore, we can derive

$$p(\vec{H}|\mathcal{D}_{\text{GW}}, \mathcal{D}_{\text{EM}}, I) \propto p_0(\vec{H}|I) \prod_i p(d_{\text{GW}}^i, d_{\text{EM}}^i|\vec{H}, I). \quad (5)$$

For a GW event, with the corresponding GW data d_{GW}^i and the EM data d_{EM}^i , the likelihood can be expressed as

$$p(d_{\text{GW}}^i, d_{\text{EM}}^i|\vec{H}, I) = \frac{\int p(d_{\text{GW}}^i, d_{\text{EM}}^i, D_L, z, \alpha, \delta, L|\vec{H}, I) dD_L dz d\alpha d\delta dL}{\beta(\vec{H}|I)}, \quad (6)$$

where α and δ represent the longitude and latitude, and L is the luminosity of the galaxy, respectively. We introduced a correction term $\beta(\vec{H}|I)$ as the denominator to eliminate the systematic biases due to selection effect [10, 35, 126]. The integrand in the numerator of Eq. (6) can be factorized as

$$\begin{aligned} & p(d_{\text{GW}}^i, d_{\text{EM}}^i, D_L, z, \alpha, \delta, L|\vec{H}, I) \\ &= p(d_{\text{GW}}^i, d_{\text{EM}}^i|D_L, z, \alpha, \delta, L, \vec{H}, I) p_0(D_L, z, \alpha, \delta, L|\vec{H}, I) \\ &= p(d_{\text{GW}}^i|D_L, \alpha, \delta, I) p(d_{\text{EM}}^i|z, \alpha, \delta, L, I) p_0(D_L, z, \alpha, \delta, L|\vec{H}, I) \\ &= p(d_{\text{GW}}^i|D_L, \alpha, \delta, I) p(d_{\text{EM}}^i|z, \alpha, \delta, L, I) p_0(D_L|z, \vec{H}, I) p_0(z, \alpha, \delta, L|\vec{H}, I). \end{aligned} \quad (7)$$

where p_0 represents the prior.

Assuming that the GW noise is Gaussian and stationary, one has [127]

$$\begin{aligned} p(d_{\text{GW}}^i|D_L, \alpha, \delta, I) &= \int p(d_{\text{GW}}^i|D_L, \alpha, \delta, \vec{\theta}', I) d\vec{\theta}' \\ &\propto \int \exp\left(-\frac{1}{2}\langle d_{\text{GW}}^i - h(D_L, \alpha, \delta, \vec{\theta}') | d_{\text{GW}}^i - h(D_L, \alpha, \delta, \vec{\theta}') \rangle\right) d\vec{\theta}', \end{aligned} \quad (8)$$

where $\langle \cdot | \cdot \rangle$ is the inner product as defined in Eq.(18), h is the waveform of the GW signal, and $\vec{\theta}'$ represents the parameters of the GW source that is unrelated to the cosmological inference. Notice that we marginalize over the parameters of the GW source that are not directly related to the constraining cosmological parameters, such as the inclination angle ι . For the dark standard siren scenario, since we assume no EM signal associated with the GW event, we set $p(d_{\text{EM}}^i|z, \alpha, \delta, L, I) = \text{const.}$ [10, 36]. We assume that $p_0(D_L|z, \vec{H}, I) \equiv \delta(D_L - \hat{D}_L(z, \vec{H}))$ under the cosmology, where $\hat{D}_L(z, \vec{H})$ is defined in Eq. (2).

In the EM observations, the sky localization of the galaxy is very accurate (relative to the sky localization of GW source), and for a galaxies catalogue from photometric sky survey, the prior $p_0(z, \alpha, \delta, L|\vec{H}, I)$ in Eq. (7) can be expressed as

$$p_0(z, \alpha, \delta, L|\vec{H}, I) = \sum_{j=1}^{N_{\text{gal}}} \left[W_j P(z|\bar{z}_j, \sigma_{z;j}) \delta(\alpha - \alpha_j) \delta(\delta - \delta_j) \left(\frac{1}{N_{\text{band}}} \sum_k^{N_{\text{band}}} P(L|\bar{L}_j^k, \sigma_{L;j}^k) \right) \right], \quad (9)$$

where N_{gal} is the total number of the galaxies catalogue, N_{band} represents the number of bands in the photometric sky surveys, and $P(x|\bar{x}, \sigma_x)$ is a Gaussian distribution on x , with expectation \bar{x} and standard deviation σ_x , $x = \{z, L\}$, and W_j is the weight of galaxy, reflect a priori confidence that the galaxy could host a compact binary. In general, although properties like metallicity, morphology, and star formation rate could be different by a lot, one can assume that the potential for each galaxy to host a compact binary is the same, i.e., $W_j = 1/N_{\text{gal}}$. However, one can alternatively expect the compact binary merger rate being proportional to the galaxy stellar mass, which is in turn related to its luminosity, and so $W_j = W(P(L_j))$, more details is described in Section IID.

Taking the above analysis into account, substituting Eq. (7) into Eq. (6) and marginalizing over the parameter D_L , Eq. (6) becomes

$$p(d_{\text{GW}}^i, d_{\text{EM}}^i | \vec{H}, I) = \frac{\int p(d_{\text{GW}}^i | \hat{D}_L(z, \vec{H}), \alpha, \delta, I) p_0(z, \alpha, \delta, L | \vec{H}, I) dz d\alpha d\delta dL}{\beta(\vec{H} | I)}. \quad (10)$$

Following the statistical method presented in [90] to evaluate the selection biases of the survey galaxies catalogue, we choose a smooth prior distribution of the catalogue redshift as

$$p_c(z | \vec{H}, I) \propto \frac{1}{2\Delta z} \int_{(z-\Delta z)}^{(z+\Delta z)} \iint_{4\pi} \int p_0(z', \alpha, \delta, L | \vec{H}, I) dL d\alpha d\delta dz', \quad (11)$$

where Δz is chosen to be much larger than the redshift interval of the galaxy clusters. The correction term $\beta(\vec{H} | I)$ in Eq. (10) can be written approximately as

$$\beta(\vec{H} | I) \approx \int p(d_{\text{GW}}^i | \hat{D}_L(z, \vec{H}), I) p_c(z | \vec{H}, I) dz. \quad (12)$$

Notice that for catalogues that is composed from multiple sources, like the GLADE catalogue [128], in order to maintain self-consistency, one need to take extra care to deal with the selection effects $p_c(z | \vec{H}, I)$ separately for different sources.

C. Localization and distance of GW source

For regular triangular space-borne GW detectors like TianQin and LISA, the recorded signal can be expressed as [74, 81]

$$h(t) = \frac{\sqrt{3}}{2} (F^+(t) h_+(t + t_D) + F^\times(t) h_\times(t + t_D)), \quad (13)$$

$$t_D \approx -\frac{R_0}{c} \sin \theta'_S \cos(\phi_d(t) - \phi'_S), \quad (14)$$

where t is the heliocentric coordinate system (HCS) time, t_D is the time delay from the solar system barycenter to the detector, $R_0 = 1\text{AU}$, the primed angles θ'_S and ϕ'_S are the altitude and azimuth of the GW source in the HCS respectively, quantities related to the source are labelled with subscript “S”, the ones related to the detector are labelled with subscript “d”. We have $\phi_d(t) = 2\pi t/T + \phi_0$, where $T = 1\text{yr}$ is the orbital period of detector around the Sun, ϕ_0 is the initial orbital phase of detector at $t = 0$. In the relatively low frequency region, $f \ll f_* = c/(2\pi L)$ (where L is the arm length of interferometer), the antenna pattern functions $F^{+, \times}(t)$ can be approximately expressed as [129]

$$F^+(t) = \frac{1}{2} (1 + \cos^2 \theta_S(t)) \cos 2\phi_S(t) \cos 2\psi_S(t) - \cos \theta_S(t) \sin 2\phi_S(t) \sin 2\psi_S(t), \quad (15a)$$

$$F^\times(t) = \frac{1}{2} (1 + \cos^2 \theta_S(t)) \cos 2\phi_S(t) \sin 2\psi_S(t) + \cos \theta_S(t) \sin 2\phi_S(t) \cos 2\psi_S(t), \quad (15b)$$

where $\theta_S(t)$, $\phi_S(t)$, and $\psi_S(t)$ are the altitude angle, the azimuth angle, and the polarization angle in the detector-based coordinate system at t . Compared with Eq. (15a, 15b), the azimuth angle of antenna pattern functions of the second independent channel differ by $+\pi/4$ for TianQin and LISA; and by $+2\pi/3$ and $+4\pi/3$ for the second and third independent laser interferometer, respectively, for ET [130]. Such difference is due to the fact that ET differs from the space-borne detectors, by using independent interferometer. The variation of $\theta_S(t)$, $\phi_S(t)$, and $\psi_S(t)$ with time depends on the motion of the detector in space, the detailed description of the detector's response to the GW signals can be found in [81, 131] for TianQin, in [132, 133] for LISA, and in [53, 134] for ET.

Notice that although in the relative high frequency range of $f \gtrsim f_*$, the low frequency limit is no longer valid for TianQin and LISA, and the sensitivity would drop in higher frequencies. It will cause some complexity for data analysis, however, as long as we absorb the effect in to the sensitivity curve, the majority of conclusions discussed in our study remain intact [76, 81, 135]. Moreover, a full analytical formulas for frequency response of space-based detector is given in [136].

Considering N independent detectors observing the same GW source, the GW signals detected by different detectors can be collectively expressed as a vector,

$$\mathbf{h} = [h_1, h_2, \dots, h_k, \dots, h_N]^T, \quad (16)$$

where h_k represents the GW strain recorded by the k -th detector. The total SNR ρ of a GW source provided by multiple independent detectors is defined as

$$\rho = \sqrt{\langle \mathbf{h} | \mathbf{h} \rangle}, \quad (17)$$

where the inner product is defined as [127, 137]

$$\langle \mathbf{h} | \mathbf{h} \rangle = \sum_k \langle h_k | h_k \rangle \equiv \sum_k 4\Re \int_0^\infty \frac{\tilde{h}_k^*(f) \tilde{h}_k(f)}{S_{n;k}(f)} df, \quad (18)$$

where $\tilde{h}_k(f)$ is the Fourier transform of $h_k(t)$, $*$ represents complex conjugate, and $S_{n;k}(f)$ is the sensitivity curve functions of the k -th detector. The sensitivity curves of TianQin [76, 81], LISA [135], and ET (ET-D) [53, 54, 138] are shown in FIG. 1.

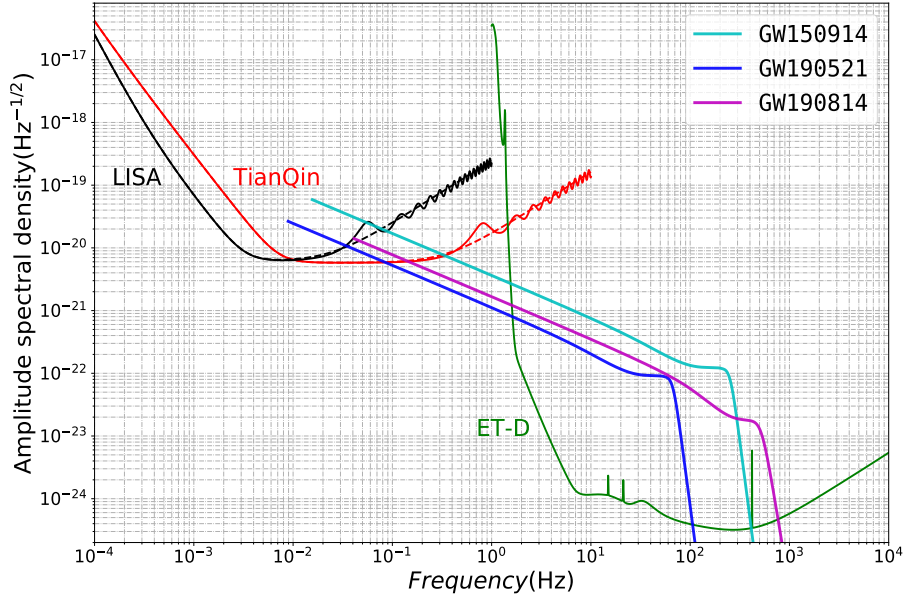


FIG. 1. Anticipated sensitivity curves for TianQin (red line), LISA (blue line), and ET-D (green line). Also shown are the amplitude spectra densities $\sqrt{f}|\tilde{h}(f)|$ of GW150914 [13] (cyan line), GW190521 [22] (blue line), and GW190814 [23] (magenta line) detected by Advanced LIGO and Virgo, assuming a 5 years merger time.

For a GW source characterized by a parameter set of $\vec{\theta} \equiv (\mathcal{M}_z, \eta, D_L, \alpha, \delta, \iota, t_c, \Psi_c, \psi)$ detected from multiple independent detectors, the Fisher information matrix (FIM) can give the Cramér-Rao lower bound on the parameter estimation uncertainty [139]. The FIM is defined as

$$\Gamma_{mn} \equiv \left\langle \frac{\partial \mathbf{h}}{\partial \theta_m} \middle| \frac{\partial \mathbf{h}}{\partial \theta_n} \right\rangle = \sum_k \left\langle \frac{\partial h_k}{\partial \theta_m} \middle| \frac{\partial h_k}{\partial \theta_n} \right\rangle, \quad (19)$$

where θ_m indicates the m -th parameter of the GW event. The covariance matrix Σ equal to the inverse of the FIM, $\Sigma = \Gamma^{-1}$, we can adopt $\Delta\theta_m = \sqrt{\Sigma_{mm}} = \sqrt{(\Gamma^{-1})_{mm}}$ as the estimation error of the parameter, with the sky localization error being $\Delta\Omega = 2\pi |\sin \delta| \sqrt{\Sigma_{\alpha\alpha} \Sigma_{\delta\delta} - \Sigma_{\alpha\delta}^2}$.

D. Galaxy weighting

If we assume that the formation rate of the SBBH per unit stellar mass is uniform across all galaxies, we can expect that the probability a galaxy hosts the SBBH is proportional to its total stellar mass.

A standard way to account for the galaxy mass is to use the K -band luminosity. It is widely accepted that the K -band traces the old stellar population of galaxies and, therefore, is approximately proportional to the galaxy stellar mass, and it is weakly correlated with the galaxy color [140, 141]. Following this logic, the K -band luminosity weighting method has been applied to the dark standard siren cosmological analysis with LIGO/Virgo data [36, 44, 49]¹.

In this work, we aim to adopt a different approach to improve the galaxy weighting process for a more accurate cosmological parameter estimation. This is achieved by deriving the galaxy stellar masses through the multi-band photometry of the galaxy samples.

1. The galaxy sample and completeness of the catalogue

For galaxy sample, we adopt the Gravitational Wave Events in Sloan (GWENS) galaxy catalogue² [44, 142], which has been assembled on purpose for the EM-GW multimessenger observations. It uses the Sloan Digital Sky Survey (SDSS) Data Release 14 (DR14) [143], which maps over 45 million galaxies that covering about a quarter of the whole sky. The GWENS catalogue provides photometric information in five bands of $ugriz$ for all galaxies, corresponding to $cModel$ magnitudes (see SDSS DR14 paper [143]) corrected for Galactic extinction from [144]. The GWENS catalogue also provides photometric redshift (photo- z) for most of the sample (about 98.5%), and spectroscopic redshifts for a small portion.

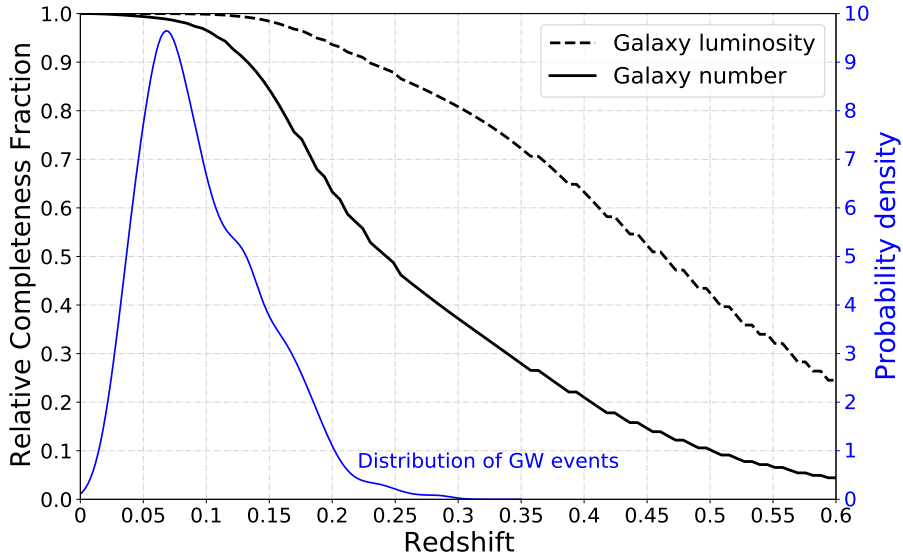


FIG. 2. The solid and dashed black lines represent completeness fractions of GWENS catalogue relative to local values, in terms of number and luminosity (in z -band), respectively. The blue line represents the probability distribution of simulated detectable GW events, with the scales shown on the right side.

In the dark standard siren study, the completeness of a galaxy catalogue plays a vital role. The relative completeness fraction of the GWENS catalogue at different redshifts are shown in FIG. 2. This is obtained by taking the galaxy luminosity distribution within $z < 0.05$ as the fiducial distribution, and by assuming that galaxies are distributed uniformly in the co-moving volume, and neglecting the evolution of the galaxy luminosity distribution with regard to redshift. Previous GW forecast studies [81] conclude that the SBBH inspirals detectable by TianQin are mainly concentrated in the range of $z < 0.2$, with the highest redshift not exceeding $z = 0.3$. The relative completeness fraction of the GWENS catalogue is about 0.63 at $z = 0.2$ and 0.37 at $z = 0.3$ from the point of view of the number of galaxies; however, from the point of view of the total luminosity contributed by galaxies, the relative completeness fraction remains above 0.9 at $z = 0.2$ and not below

¹ The B -band luminosity information is also used, which reflects the star formation rate of galaxy.

² The GWENS is available at: https://astro.ru.nl/catalogs/sdss_gwgalcat

0.8 at $z = 0.3$. These levels of relative completeness fraction ensures that most host galaxies for GW sources is within the list, and the GWENS catalogue can meet our requirement. Notice there exist other galaxy catalogues, like the GLADE catalogue [128] and the DES catalogue [145–147], but we settled with the GWENS catalogue for higher completeness and for larger sky coverage.

2. Stellar masses

Galaxy masses are derived using a standard spectral energy distribution (SED) fitting software, **Le Phare** ([148, 149]). **Le Phare** matches the observed galaxy colours with the colours predicted from a set of theoretical SED libraries from simple stellar population (SSP) models, characterized by a series of stellar parameters like age τ , metallicity Z , and a star formation history. The SED are convolved with the filter transmission curves (including instrument efficiency) adopted for the specific observation dataset to derive synthetic luminosities in the adopted bands. The best-fit parameters are obtained via χ^2 minimisation between the synthetic colours SED and photometric data. The input data are constituted by the multi-band photometric magnitudes from the GWENS catalogue [44, 142], the output are the best stellar population parameters, including the age, metallicity, star formation rate and the stellar mass. For the SSP models we adopt stellar templates from [150] with an initial mass function (IMF) [151] and an exponentially decaying star formation history. We use a broad set of models with three metallicities ($0.005Z_\odot$, Z_\odot , and $2.5Z_\odot$) and different ages ($\tau \leq \tau_{\max}$), with the maximum age, τ_{\max} , set by the age of the Universe at the redshift of the galaxy, with a maximum value at $z = 0$ of 13.5 Gyr. We also consider internal extinction using the models from [152]. Finally, to reduce the degeneracies between the redshift and galaxy colours, in the **Le Phare** run we fix the galaxy redshift to the median of probability density function (PDF) of photo- z reported in the GWENS catalogue. The final distribution of the stellar masses for the 45 141 307 GWENS galaxies is shown in FIG. 3. The stellar masses cover a rather large range, from dwarf-like systems ($\sim 10^7 M_\odot$) to massive galaxies ($\sim 10^{12}$), as well as a large range in redshifts (from 0 to ~ 0.8).

To check the presence of biases in our mass estimates, we compare them with stellar masses obtained for SDSS DR 12 (Portsmouth SED-fit Stellar Masses, this is the catalog of stellar masses of 1 489 670 systems from the Portsmouth Group³, see also [153]), for which we have found an overlap of $\sim 53\,700$ galaxies with GWENS. We evaluate the mean deviation between our estimates and the SDSS “starburst model” catalogue to be $\Delta_M = 0.14$ and scatter $\sigma_M = 0.32$, meaning that the two stellar mass estimates are basically consistent with each other (note that in case we compared against the Portsmouth passive model catalogue we obtain $\Delta_M = -0.07$ and scatter $\sigma_M = 0.18$). The scatter obtained by these comparison is reasonably small considering the rather different models adopted in the two approaches (e.g. [154] and [155] templates, no reddening and a different magnitude definition).

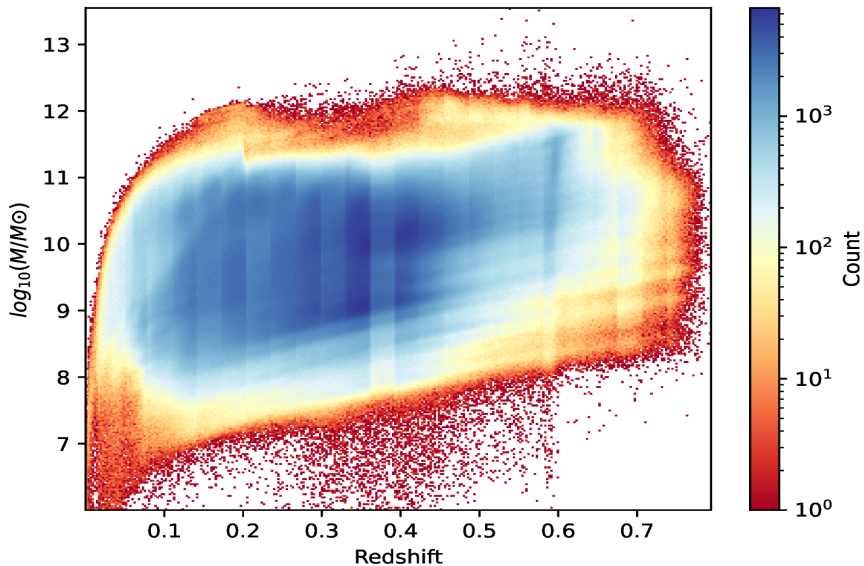


FIG. 3. Distribution of total stellar masses for GWENS galaxies derived from the **Le Phare** method. Note that the redshift in horizontal coordinates represents the median of the posterior probability distribution of the photo- z of galaxies.

³ Available at: https://www.sdss.org/dr12/spectro/galaxy_portsmouth/

III. SIMULATIONS

In order to quantitatively analyse the constraint of the Hubble constant by GW signals with the future space-borne and ground-based GW detectors, we first simulate a GW event catalogue, then select out candidate host galaxies according to the spatial localization of GW source, and finally obtain their statistical redshift information.

A. Stellar-mass black hole binary signals

We adopt the ‘Power Law + Peak’ model to populate the SBBH simulation [156]. Based on the 50 GW events published by the first (GWTC-1) [19] and the second Gravitational-Wave Transient Catalog (GWTC-2) [24], this mode is associated with the highest Bayesian factor. The model is composed with a power-law mass distribution for the primary component, with a smooth truncation at the lower mass limit, added with a Gaussian peak at the high mass end to account for the pile-up effect of pulsational pair-instability supernovae [156, 157]. The mass ratio q which describes the ratio between the secondary component mass and the primary component mass, is modeled by a power law [158–160], $p(q|m_1) \propto q^{\beta_q}$, and $\beta_q = 1.3^{+2.4}_{-1.6}$ [156]. According to [156], we adopt the associated SBBH merger rate as $R_{\text{SBBH}} = 58^{+54}_{-29} \text{Gpc}^{-3} \text{yr}^{-1}$ ⁴, which assumes that $m_1 \geq 2M_\odot$ and including GW190814.

Moreover, we ignore the spins of inspiralling SBBH, because the black hole spin effect has negligible effect on the GW cosmology study [161, 162]. The eccentricity of the SBBH, which is not well constrained by LIGO and Virgo observation, but should have non-negligible effects for space-borne GW detections. Throughout this work, we set the eccentricity to $e_0 = 0.01$ at GW frequency equal to 0.01 Hz as a representative value [81, 162].

Furthermore, we assume that SBBHs are uniformly distributed in the co-moving volume. Each GW event is randomly host in a galaxy of the GWENS catalogue, and assuming that the probability of each galaxy being hosted by a GW event is proportional to its total stellar mass. The distribution of orientation parameters are chosen to be isotropic, i.e., $\alpha \in \text{U}[0, 2\pi]$, $\cos \delta \in \text{U}[-1, 1]$, $\alpha_L \in \text{U}[0, 2\pi]$, and $\cos \delta_L \in \text{U}[-1, 1]$; the spins are fixed at $\chi_{1,2} \equiv 0$; the remaining parameters are assumed to obey uniform distribution, $t_c \in \text{U}[0, 20] \text{yr}$, and $\Phi_c \in \text{U}[0, 2\pi]$. Finally, we produce the simulated GW signals with the IMRPhenomPv2 waveform [163].

B. Detections with GW detectors

In this work, we consider multiple detector configurations with space-borne and the ground-based GW detectors, as described below,

- *TianQin*: the default case with three satellites form a constellation and operate in a “3 month on + 3 month off” mode, with a mission life time of 5 years [72];
- *TianQin I+II*: a twin constellations of satellites with perpendicular orbital planes, operate in a relay mode and can avoid the 3 months gap in data [76, 81, 164];
- *TianQin+LISA*: a multi-detector GW detector network of TianQin and LISA, we adopt LISA configurations according to [73, 135], and considering 4 years of overlap in operation time;
- *TianQin I+II+LISA*: similar to above but with the TianQin I+II configuration considered;
- *TianQin+ET*: a multi-band GW detector network of TianQin and ET, with 5 years of overlap in operation time, we adopt ET configurations according to [52, 54, 138], and assumed to continue operating for 15 years after the end of TianQin mission;
- *TianQin I+II+ET*: similar to TianQin+ET but with the TianQin I+II configuration considered.

In TABLE I, we list the anticipated detection rates with respect to different detection thresholds for SBBH inspirals that merge within 20 years from the start of TianQin detection. Throughout this work, we adopt two SNR thresholds for different detector configurations, one with $\rho_{\text{thre}} = 8$ for space-borne GW detectors [80, 81], including TianQin, TianQin I+II, TianQin+LISA and TianQin I+II+LISA; and the other with $\rho_{\text{thre}} = 5$ for multi-band GW detections [99, 102], such as TianQin+ET and TianQin I+II+ET. It is worth mentioning that, for sources with $\rho \geq 5$ detected with space-borne GW detectors/networks, they can all be detected by ET with

⁴ Notice that a revised version reports an updated value of $R_{\text{SBBH}} = 52^{+52}_{-26} \text{Gpc}^{-3} \text{yr}^{-1}$.

TABLE I. Total detection rate of the SBBHs with $t_c < 20\text{yr}$ over the entire observation time that based on the ‘Power Law + Peak’ SBBH population model for five detector configurations: TianQin, TianQin I+II, LISA, TianQin+LISA and TianQin I+II+LISA.

SNR	Total detection rate				
Threshold	TianQin	TianQin I+II	LISA	TianQin+LISA	TianQin I+II+LISA
$\rho \geq 5$	$44.2^{+43.1}_{-21.1}$	$111.6^{+108.1}_{-53.3}$	$74.2^{+70.3}_{-36.2}$	$155.9^{+147.4}_{-75.7}$	$245.8^{+234.9}_{-120.1}$
$\rho \geq 8$	$10.8^{+10.1}_{-5.5}$	$28.4^{+26.0}_{-14.9}$	$16.8^{+16.7}_{-8.2}$	$38.3^{+36.1}_{-19.4}$	$63.8^{+58.7}_{-32.7}$
$\rho \geq 12^a$	$3.0^{+3.1}_{-1.4}$	$7.8^{+7.8}_{-3.6}$	$4.6^{+4.6}_{-1.9}$	$10.6^{+9.9}_{-5.2}$	$17.5^{+17.6}_{-8.5}$

^a A conservative SNR threshold [81].

$\rho \gtrsim 20$, as long as ET is operating when they merge. Therefore we do not list ET in TABLE I, and we do not consider GW sources that can only be detected by ET in this work.

The precision of the Hubble constant constrained by GW signals of SBBH mainly depend on the spatial localization errors of the GW sources. In FIG. 4, we illustrate the marginalised distribution on relative error of luminosity distance σ_{D_L}/D_L and sky localization $\Delta\Omega$. Since the GW events are useful for reconstructing the $D_L - z$ relation only when the luminosity distance can be decently estimated, we only include GW sources with $\sigma_{D_L}/D_L < 0.6$ (approximately corresponding to $\Delta D_L/D_L < 1$ at the confidence level of 90%) to consideration in this work.

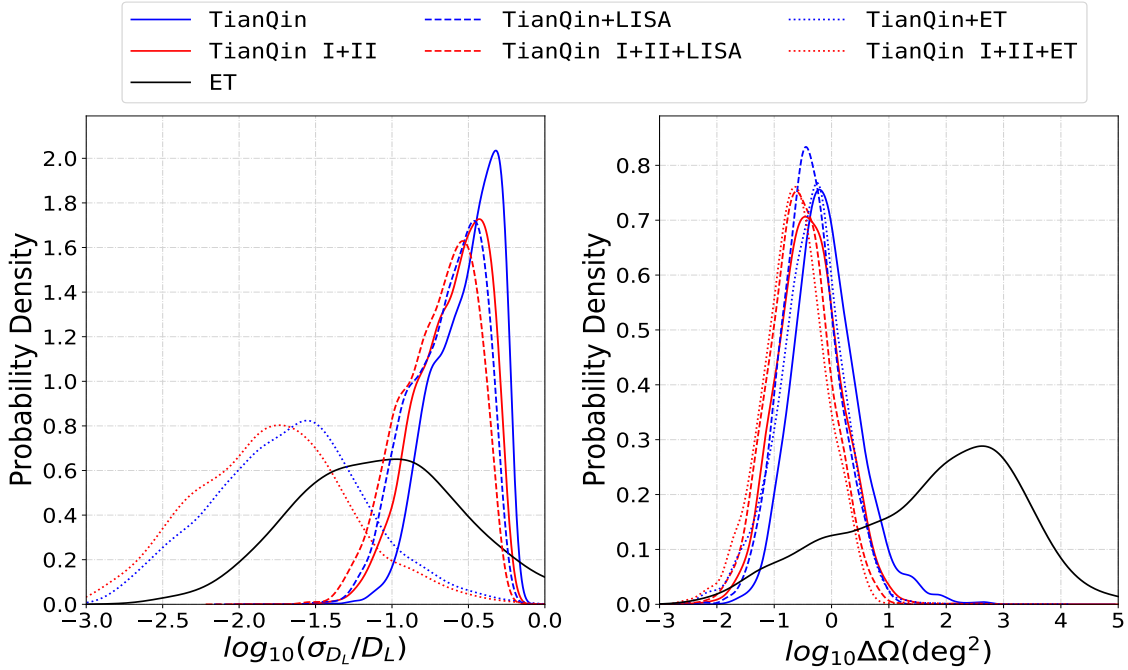


FIG. 4. Spatial localization error distribution for TianQin (solid blue line), TianQin I+II (solid red line), TianQin+LISA (dashed blue line), TianQin I+II+LISA (dashed red line), TianQin+ET (dotted blue line), TianQin I+II+ET (dotted red line), and ET (solid black line).

We notice that for events detected by TianQin or TianQin I+II, the relative error of luminosity distance for most GW sources are greater than 0.1, but the sky position of most GW sources can be localised to better than 1deg^2 . The network of TianQin (or TianQin I+II) and LISA can marginally improve the spatial localization of the GW sources. This is because that TianQin has better sensitivity in higher frequencies compared with LISA, which is where the SBBH inspiral signals concentrate.

On the other hand, for events detected by ET, due to the time-dependent modulation of antenna beam-pattern related to the Earth rotation, a typical sky localization error is at the level of $10^2 \sim 10^3\text{deg}^2$. Notice that there is a strong degeneracy between sky localization and luminosity distance, because the polarization angle of a GW signal depends on the relative position between the GW source and the detector, such large sky localization error

leads to a large uncertainty on polarization, which translates into a large uncertainty of inclination angle, and finally also on luminosity distance. Although most GW signals detected by ET have high SNRs (on the order of $10^2 \sim 10^3$), the typical relative error on the luminosity distance is about 0.1.

One remarkable conclusion we can draw from FIG. 4 is that the multi-band GW detection can significantly improve the estimation precision of luminosity distance. GW detection from space-borne detector(s), can provide a very precise sky localization, which then breaks the degeneracy between the sky localization and the luminosity distance for the ground-based detector(s). The relative error on luminosity distance can be improved by one order of magnitude compared with TianQin/LISA, and by half order of magnitude compared with ET.

C. Statistical redshift

The spatial localization information of GW source cannot be used directly to select potential host galaxies of the GW source. The possible range of luminosity distance $[D_L^-, D_L^+] \equiv [(\bar{D}_L - 2\sigma_{D_L}), (\bar{D}_L + 2\sigma_{D_L})]$ (where \bar{D}_L is the mean value) needs to be converted into the possible range of redshift $[z^-, z^+]$ first. The candidate host galaxies are then selected from the survey galaxy catalogue according to the error box of redshift-space. This conversion depends on both a specific cosmological model and the prior of the corresponding cosmological parameters. We convert the luminosity distance range into the redshift possible range under the standard Λ CDM model, with the prior of $H_0 \in \mathcal{U}[30, 120]$ km/s/Mpc and $\Omega_M \in \mathcal{U}[0.04, 0.6]$. The conversion relation is given by

$$D_L^- = c(1 + z^-) \int_0^{z^-} \frac{1}{H^-(z')} dz', \quad (20a)$$

$$D_L^+ = c(1 + z^+) \int_0^{z^+} \frac{1}{H^+(z')} dz', \quad (20b)$$

where $H^-(z)$ and $H^+(z)$ are the specific realizations of Hubble parameter that minimize and maximize Eq. (1) within the prior of both H_0 and Ω_M .

In our simulation, we obtain the candidate host galaxies of the GW source from the GWENS catalogue. To properly account for the redshift uncertainty, we consider two factors: (1) the redshift information of galaxy in the catalogue is almost all photo- z , including non-negligible photo- z error Δz_{photo} ; (2) due to the peculiar velocity of galaxies, the observed spectroscopic redshift z_{obs} is different from the cosmological redshift z , and we denote this redshift error $\Delta z_{\text{pv}} \equiv |z_{\text{obs}} - z|$. In general, $\Delta z_{\text{photo}} \gg \Delta z_{\text{pv}}$, so the final boundary of redshift of candidate host galaxies is defined as $[z_{\text{min}}, z_{\text{max}}] = [(z^- - \Delta z_{\text{photo}}), (z^+ + \Delta z_{\text{photo}})]$. The final spatial localization error box of candidate host galaxies is defined by $4\Delta\Omega \times [z_{\text{min}}, z_{\text{max}}]$ (the factor of 4 corresponds to the 2σ confidence level for the GW sky localization). For a small number of galaxies with spectroscopic redshift, we discard Δz_{photo} and approximate $\Delta z_{\text{pv}} \approx (1 + z_{\text{obs}})\langle v_p \rangle / c$, assuming $\langle v_p \rangle = 500$ km/s [165]. The impact of peculiar velocities and their reconstruction on the estimation of H_0 has been studied in Refs. [165–168], and it is possible to eliminate the redshift error Δz_{pv} for nearby galaxies.

For each galaxy in the GW error box, we adopt the following two methods to obtain the statistical redshift:

- *fiducial method*: assigning equal weight regardless of its position and luminosity;
- *weighted method*: assigning a weight that accounts both its positional and luminosity-related information.

When the sky localization from GW detection is described by a covariance matrix $\Sigma_{\alpha\delta}$, the positional weight of a galaxy at location (α_j, δ_j) is defined as $W_{\text{posi}} \propto \exp \left\{ -\frac{1}{2} \left[(\alpha_j - \bar{\alpha}, \delta_j - \bar{\delta}) \Sigma_{\alpha\delta}^{-1} (\alpha_j - \bar{\alpha}, \delta_j - \bar{\delta})^T \right] \right\}$, where $(\bar{\alpha}, \bar{\delta})$ are the best measured values of the sky localization. Meanwhile, we assign the luminosity-related weight as proportional to the derived total stellar mass of the galaxy, which is derived from the photometric information through the **Le Phare** software (see Section IID for details).

FIG. 5 illustrates an example localization of a SBBH GW signal, and how different weighting methods as well as redshift (photometric or spectroscopic) can impact on the final redshift estimation of the SBBH. The sky localization of GW source is generally too uncertain to uniquely identify host galaxy without an EM counterpart, more accurate sky localization can eliminate the interference of many polluting galaxies. The left panel shows the advantage of more accurate sky localization of TianQin I+II over TianQin in selecting the galaxies; the middle panels shows the different distributions of the statistical redshifts under the two detector configurations, one can conclude that fewer candidate host galaxies make the redshift of the true host galaxy more significant. In addition, the distribution of redshift based on photometric data appears to be more smooth due to large photo- z error, while the distribution based on spectroscopic data shows larger fluctuation, which leads to better potential of constraining the Hubble constant. Notice that since the quality of the statistical redshift distribution for the host galaxy depends mainly on the spatial localization precision from the GW detection, we do not repeat the above calculation on other configurations as the sky localization is not significantly different.

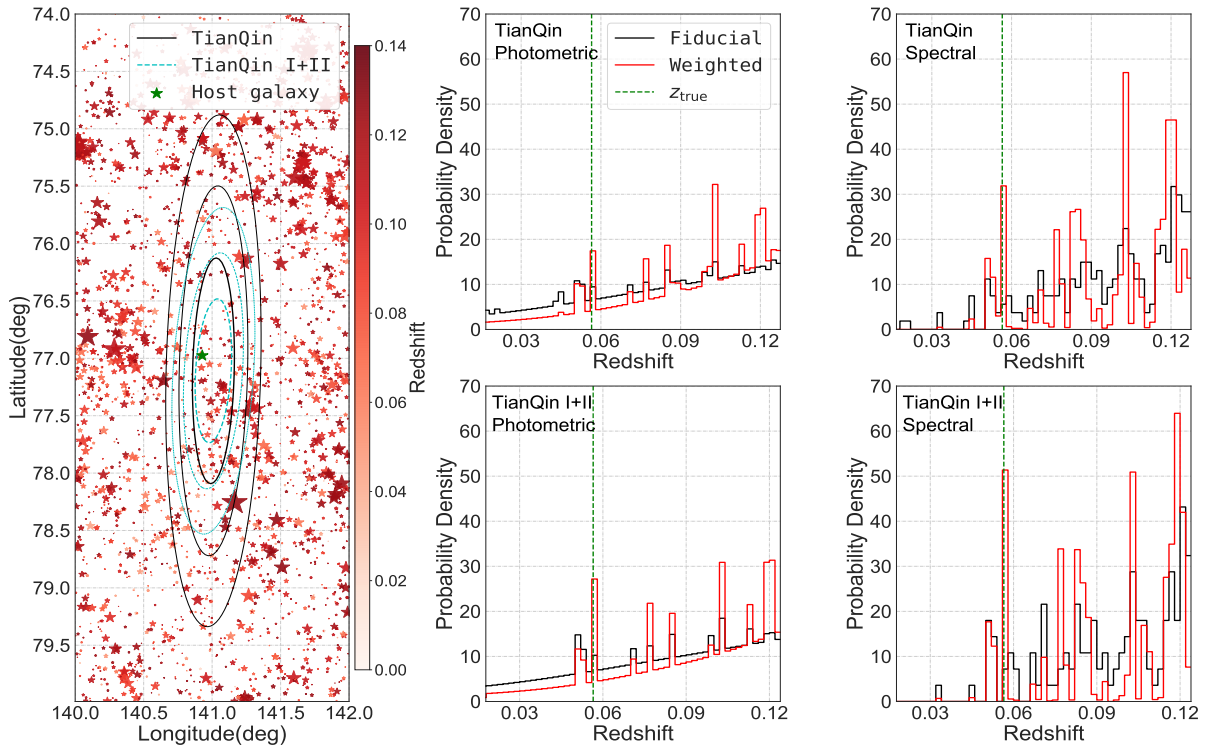


FIG. 5. Sky localization and statistical redshift distribution of an example SBBH inspiral. The left panel shows sky localizations of both TianQin (solid black contour lines) and TianQin I+II (dashed cyan contour lines) and a scatter plot of galaxies within the catalogue, the green star labels the real host galaxy; the shade of star represents its redshift, and the size of star represents its luminosity-related weight. The middle panels show the statistical photo- z of TianQin (top) and TianQin I+II (bottom), respectively, using two statistical redshift estimation with both the fiducial method (black histograms) and the weighted method (red histograms), and the vertical green dashed line represents the true redshift of the GW source. The right panels show the same as middle panels but with spectroscopic galaxy redshifts.

It is slightly counter-intuitive that better sky localization might lead to a worse redshift estimate. This is because the photo- z estimate for any single galaxy is usually accompanied with a relatively large random error. When the GW signal is localised to a larger area, more galaxies are involved, and the intrinsic clustering of galaxies effectively average out the random error. On the other hand, for better sky localizations, such averaging is less effective. However, we anticipate that future detections would trigger passion on a comprehensive survey of galaxies within the GW error box. Therefore, we expect for events that can be localised to an area smaller than $\Delta\Omega < 0.1\text{deg}^2$, spectroscopic redshift would be available for galaxies with apparent magnitude $m_{\text{app}} \leq +21\text{mag}$ [169]. In practice, we simply adopt the median value of the photo- z as the “true value” of the spectroscopic redshift.

IV. RESULTS

We use a Markov chain Monte Carlo (MCMC) algorithm — `emcee` package, which is a Python implementation of an affine-invariant MCMC ensemble sampler [170, 171], to extract the Hubble constant from the dark standard sirens. In FIG. 6, we illustrate an example of cosmological parameters estimation with TianQin I+II. We demonstrate that although single event might suffer from large uncertainties for not identifying the host galaxy, a number of events can cancel out the random error and lead to a more precise estimate of the Hubble constant.

Because of the uncertainty related to the luminosity distance, the redshift (Δz_{photo} and Δz_{pv}), and the cosmological model, one GW event can often be associated with many galaxies with a wide range of redshifts (see Eq. (20a, 20b)), shown as the horizontally distributed dots in FIG. 6. After constraining cosmological parameters, the redshift range of candidate host galaxies of GW source will be considerably reduced, which is referred to as the posterior redshift. The candidate host galaxies within the posterior redshift finally determine the constraint precision of cosmological parameters, the other candidate host galaxies outside the posterior redshift are just interference sources, but we cannot exclude them when the cosmological parameters are not constrained.

In this section, we report the results of constraints on H_0 with SBBH GW signals under different detector

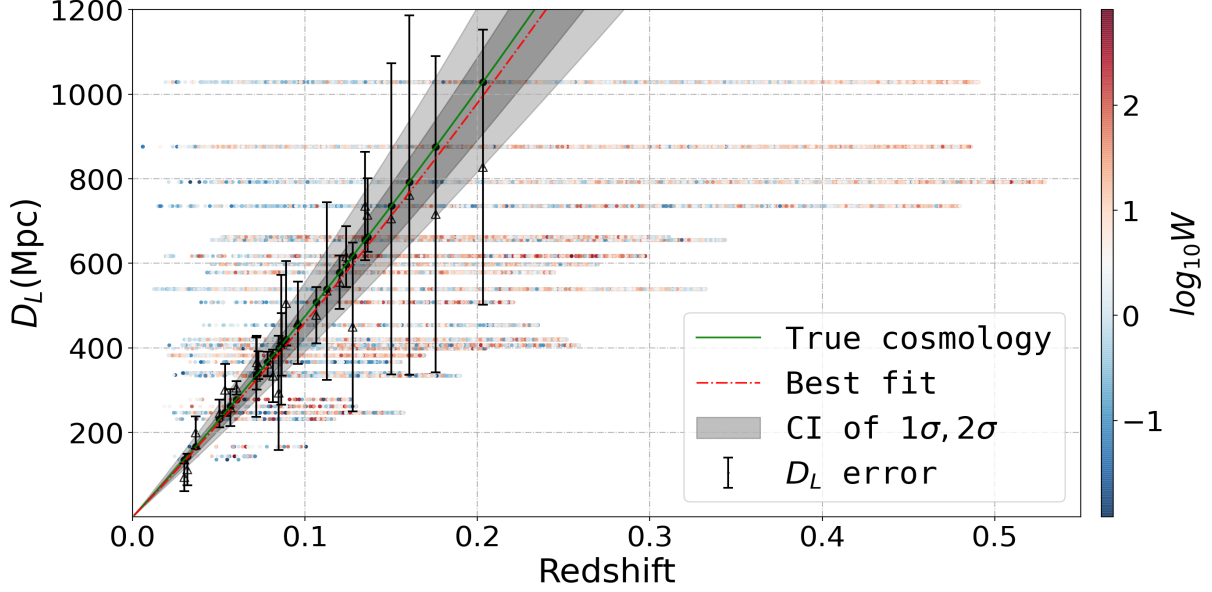


FIG. 6. An example of the $D_L - z$ relation with TianQin I+II dark standard siren observation. The solid green line represents injected cosmological parameters H_0 and Ω_M . The dotted-dashed red line represents the most probable cosmology, and the two shaded areas represent 68.27% (1σ) and 95.45% (2σ) confidence intervals, respectively. The black error bars represent measurement errors of luminosity distance to GW sources. In each error bar, the median hollow black triangles represent the mean value of D_L measurement with random statistical deviation, and the solid black dot represents the true value of D_L . The horizontal coloured dots represent the redshift of selected galaxies for that particular source, the colors ranging from blue to red show the logarithms of the total weights of galaxies, and we assigned to D_L of each candidate host galaxy equal to the true D_L of the GW source.

configurations, i.e., TianQin, TianQin I+II, TianQin+LISA, TianQin I+II+LISA, TianQin+ET, and TianQin I+II+ET. In order to alleviate the effect raised by any random realisation, for each configuration, for all calculation, we repeat the calculation on 48 random realizations with different random seeds. Also, when reporting the constraining on H_0 , the result is marginalized over Ω_M , instead of fixing a specific Ω_M value.

A. TianQin and TianQin I+II

The current studies of the population properties of SBBH merger events observed by LIGO and Virgo have revealed a large uncertainty for the merger rate of SBBH [19, 24, 156, 158], which also leads to a large uncertainty in the prediction of the detection rate of GW events from SBBHs. In order to avoid the influence of the detection rate of GW events on the constraint precision of H_0 and entirely display the potential of detector(s), we studied variation of the constraint precision of H_0 with the number of GW events in detail, varying from 6 to 120 events. The constraints on H_0 for TianQin and TianQin I+II are shown in FIG. 7. The uncertainty of H_0 shrinks as the number of detected GW events increases. Compared with the fiducial method, the weighted method can improve the constraining precision of H_0 by a factor of about 2.

TianQin can detect about 11 SBBH GW events over 5 years of operation (as illustrated in TABLE I), with which, one can constrain H_0 to a precision of about 36.8% using the fiducial method and about 30.9% using the weighted method, respectively. Due to the small number of GW events, the constraints of cosmological parameters are very imprecise, a typical constraint result of the parameters h ($h \equiv \frac{H_0}{100 \text{ km/s/Mpc}}$) and Ω_M from TianQin using the weighted method is shown in the left plot of FIG. 8.

From FIG. 7, one can find that the constraint on H_0 with TianQin I+II is tighter than that with TianQin. Given the same number of GW events and the weighting method of candidate host galaxies, TianQin I+II can significantly improve the constraint of H_0 . This improvement is mainly due to the more accurate spatial localization with TianQin I+II, as shown in to FIG. 4. For TianQin I+II, about 28 GW events are expected to be detected, and the precision of H_0 is expected to be about 26.3% and about 14.4% using the fiducial method and the weighted method, respectively. A typical cosmological parameter estimation using weighted method for TianQin I+II are shown in the right plot of FIG. 8. Thanks to higher GW detection rate and more accurate spatial localization of GW sources, the non-Gaussian tail of the posterior probability distribution of H_0 becomes shorter. For Ω_M , there are no effective constraints by using SBBH GW events, either for TianQin or TianQin

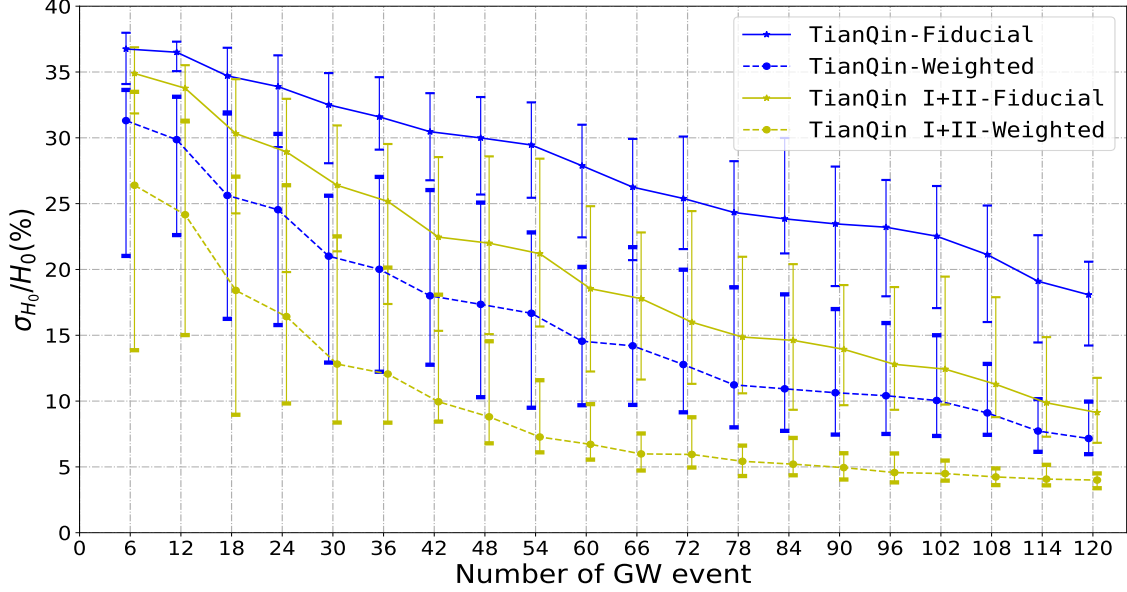


FIG. 7. Dependence of constraint precision of H_0 on numbers of GW events for TianQin (blue) and TianQin I+II (yellow). The fiducial method and the weighted method are shown in solid and in dashed line, respectively. Each error bar represents 68.27% interval from 48 independent simulations. Lines are slightly shifted for better visual presentation.

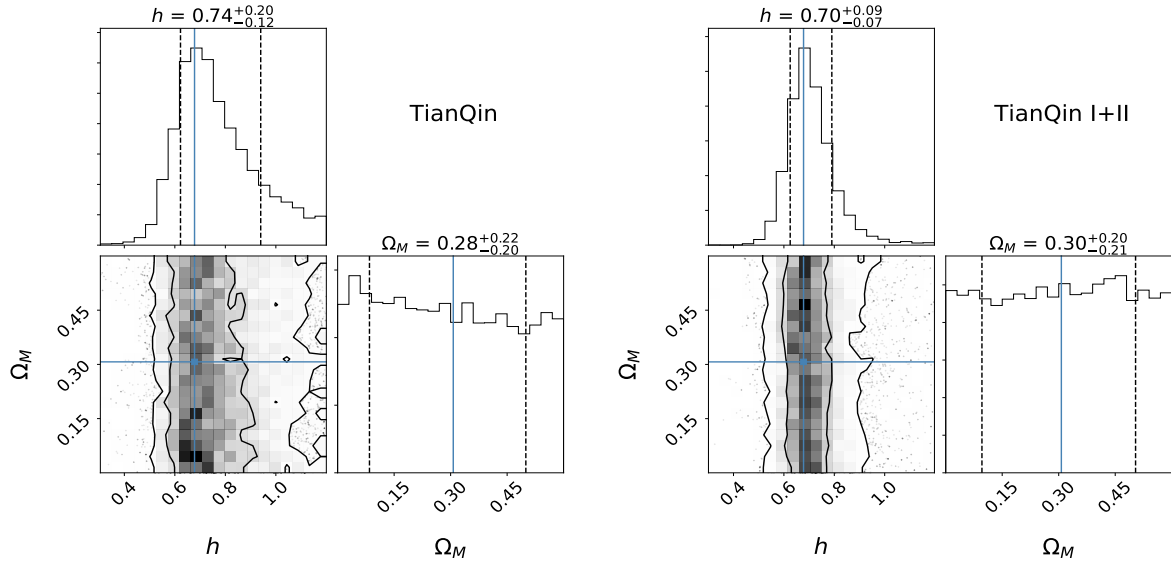


FIG. 8. Examples of the posterior probability of the parameters h and Ω_M using the weighted method for TianQin (left) and TianQin I+II (right). In each plot, the lower left panel shows the joint posterior probability of h and Ω_M , with the contours represent confidence levels of 1σ (68.27%) and 2σ (95.45%), respectively; the upper and right panels show the marginalised posterior distribution of same parameters, with the dashed lines indicate 1σ credible interval. In each panel the solid cyan lines mark the true values of the parameters.

I+II.

It is worth noting that the precision of H_0 with TianQin under the weighted method is higher than that from TianQin I+II by the fiducial method, indicating that compared with better spatial localization, a better weighting method has a larger impact on the H_0 estimation.

B. Multi-detector network of TianQin and LISA

We then consider the cases when LISA is added to the detector network. In FIG. 9, we show the dependence of the precisions of H_0 versus detection numbers, assuming TianQin+LISA and TianQin I+II+LISA. We observe

again that more detections lead to more precise H_0 measurement. In FIG. 10, we present a typical joint probability of h and Ω_M using the weighted method under the expected total detection rates (see TABLE I for details). We notice that TianQin+LISA has very similar constraining power to that of TianQin I+II, because the two detection configurations have very similar localization precisions (see FIG. 4). Meanwhile, TianQin I+II+LISA can half the uncertainty on H_0 , again due to better localization. However, neither of the two detector network configurations has meaningful constraint on Ω_M .

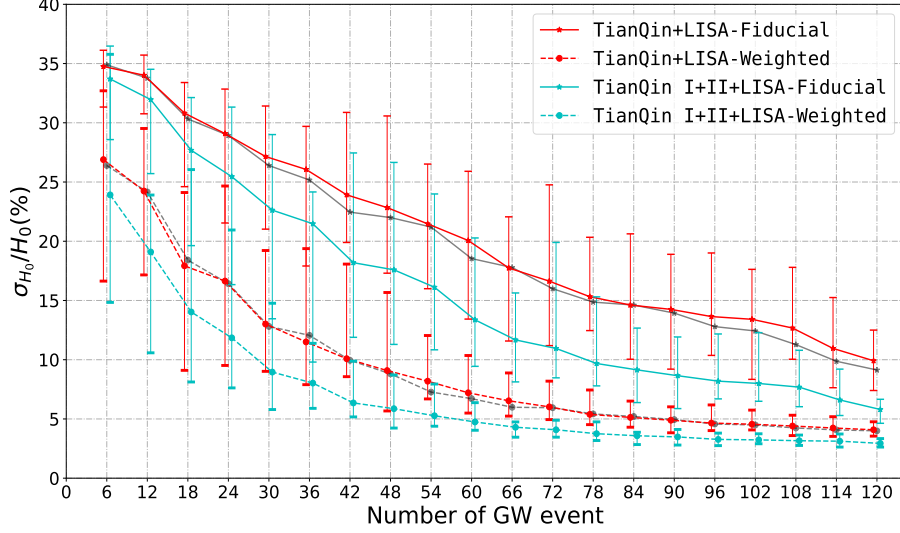


FIG. 9. Dependence of constraint precision of H_0 on numbers of GW events for TianQin+LISA (red) and TianQin I+II+LISA (cyan). The fiducial method and the weighted method are shown in solid and in dashed line, respectively. Each error bar represents 68.27% interval from 48 independent simulations. The similar results of TianQin I+II (gray) are also shown for comparison. Lines are slightly shifted for better visual presentation.

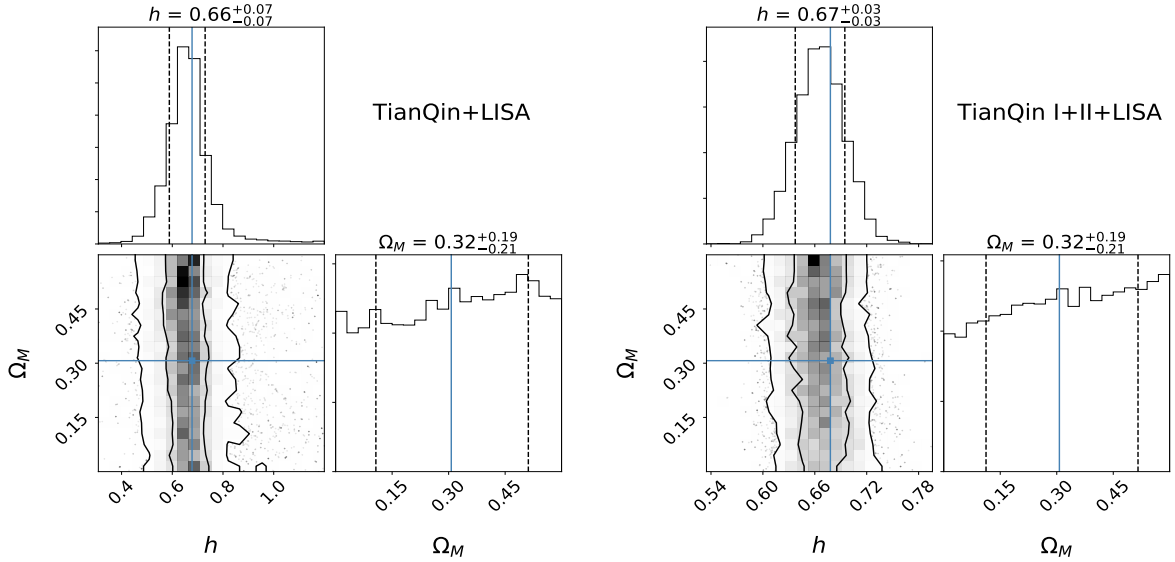


FIG. 10. Examples of the posterior probability of the parameters h and Ω_M using the weighted method for TianQin+LISA (left) and TianQin I+II+LISA (right). In each plot, the lower left panel shows the joint posterior probability of h and Ω_M , with the contours represent confidence levels of 1σ (68.27%) and 2σ (95.45%), respectively; the upper and right panels show the marginalised posterior distribution of same parameters, with the dashed lines indicate 1σ credible interval. In each panel the cyan lines mark the true values of the parameters.

For TianQin+LISA (TianQin I+II+LISA), about 38 (64) GW events are expected to be detected, and the precision of H_0 can be constrained to about 25.2% (12.2%) and about 11.6% (4.1%) by using the fiducial method and the weighted method, respectively. Similar to the case of TianQin and TianQin I+II, the constraint of H_0 by TianQin+LISA using the weighted method is stronger than that by TianQin I+II+LISA using the fiducial

method.

The space-borne GW detectors/networks have excellent sky localizing capability, which empowers the constraints on Hubble constant through the observation of SBBH inspirals. However, such SBBH inspiral GW signals are relatively quieter, the relatively lower SNR leads to a larger uncertainty on luminosity distance, $\sigma_{D_L}/D_L \gtrsim 0.1$. This fact restricts the expected precision of H_0 from the SBBH inspiral observation with the space-borne detectors.

C. Multi-band detection with TianQin and ET

A multi-band GW observation of SBBH can provide a significant improvement in constraining the Hubble constant under the dark standard siren scenario, since the multi-band observation combines advantages of both space-borne and ground-based detectors. The space-borne GW detectors can provide accurate sky localization, while the high SNR contributed by the ground-based detectors result in a more precise luminosity distance estimation. Such combination leads to a smaller error box, which can be less disturbed by other contaminating galaxies and eventually provides a more precise estimation of the redshift.

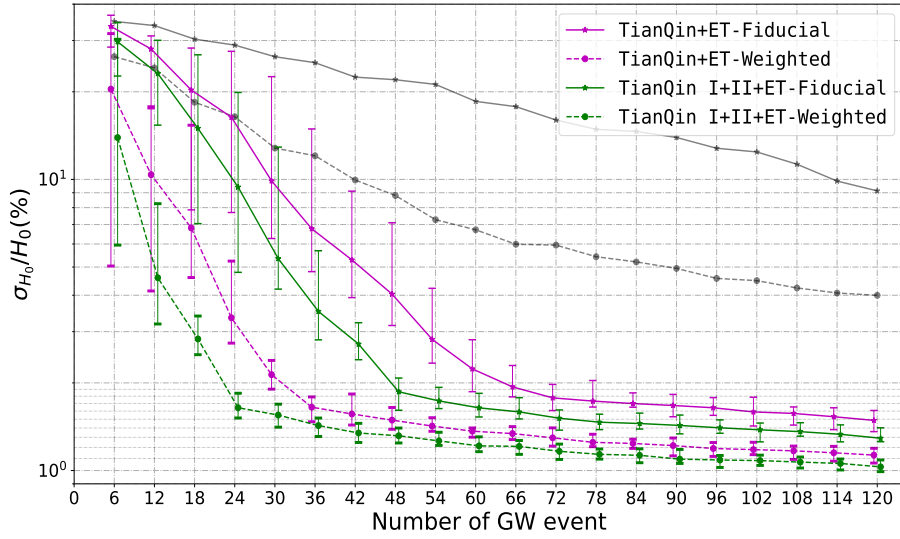


FIG. 11. Dependence of constraint precision of H_0 on numbers of GW events for TianQin+ET (magenta) and TianQin I+II+LISA (green). The fiducial method and the weighted method are shown in solid and in dashed line, respectively. Each error bar represents 68.27% interval from 48 independent simulations. The similar results of TianQin I+II (gray) are also shown for comparison. Lines are slightly shifted for better visual presentation.

In FIG. 11, we present the dependence of constraint precision of H_0 versus different detection numbers, under the multi-band GW detector networks TianQin+ET and TianQin I+II+ET. Notice that the TianQin I+II lines (gray) roughly follows a power-law relation, while the lines for multi-band networks indicates a saturation from relative uncertainties around 1.8%, which also corresponds to a turning point for the trend of the lines, respectively. We observe that the multi-band network can quickly increase the precision of H_0 as more events are observed, but after the turning point, the precision improves only by $1/\sqrt{N}$, where N is the number of GW events. And the precision is hardly to reach the level of 1% even after 100 GW events are detected. We also notice that when adopting the weighted method, the better precision leads to a quicker approaching of the saturation, which happens at around 24 events for the TianQin I+II+ET network.

For TianQin+ET, about 44 GW events are expected to be detected through multiple band observation (as illustrated in TABLE I), and the precision of H_0 can be constrained to about 4.7% and about 1.5% by using the fiducial method and the weighted method, respectively. Moreover, if TianQin I+II+ET is realized, about 112 GW events can be detected through multi-band observations in the optimistic case, and the precision of H_0 can be constrained to $\sim 1\%$, either using the fiducial method (about 1.3%) or using the weighted method (about 1.1%). Constraining H_0 to a precision of 1% would be very exciting as it has the potential to shed light on the Hubble tension.

The typical constraints on h and Ω_M using the weighted method for the multi-band networks are shown in FIG. 12. The introduction of multi-band GW observation can greatly enhance the constraining power on cosmological parameter Ω_M . Although the fiducial method does not deliver significant and robust estimation, the weighted

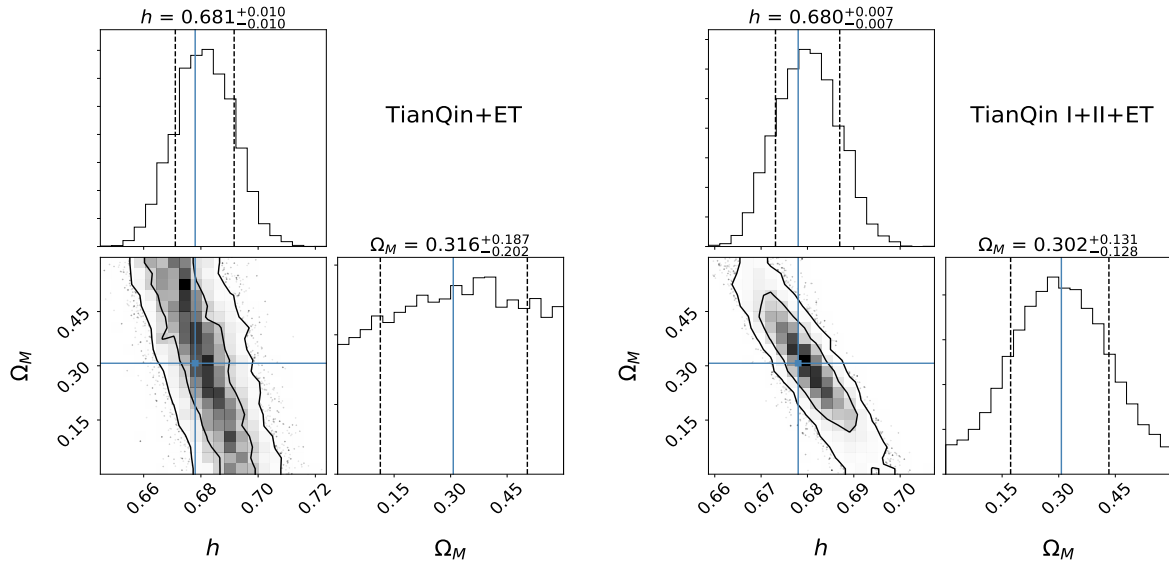


FIG. 12. Examples of the posterior probability of the parameters h and Ω_M using the weighted method for TianQin+ET (left) and TianQin I+II+ET (right). In each plot, the lower left panel shows the joint posterior probability of h and Ω_M , with the contours represent confidence levels of 1σ (68.27%) and 2σ (95.45%), respectively; the upper and right panels show the marginalised posterior distribution of same parameters, with the dashed lines indicate 1σ credible interval. In each panel the cyan lines mark the true values of the parameters.

method can constrain Ω_M to a precision of 0.13, or equivalently 42% for relative uncertainty, with the TianQin I+II+ET network.

V. DISCUSSIONS

A. Important role of spectroscopic redshift

Considering that the sky localization error of almost all GW sources is less than 10 deg^2 , it might be possible to use current or future spectroscopic observation facilities, like the Large Sky Area Multi-Object Fiber Spectroscopic Telescope (LAMOST) [172–174], the Dark Energy Spectroscopic Instrument (DESI) [175], the 4-meter Multi-Object Spectroscopic Telescope (4MOST) [176], the TAIPAN [177], the Chinese Space Station Telescope (CSST) [169], the James Webb Space Telescope (JWST) [178, 179], and the Wide-Field InfraRed Survey Telescope (WFIRST) [180, 181], to perform galaxy survey and provide accurate estimation for the galaxies locate in the error box. In this section, we investigate to which extent a catalogue of galaxies with spectroscopic redshifts can improve the constraint precision of H_0 . TABLE II summarises the constraint precision of H_0 under various detector configurations, and under two assumptions that the survey galaxy catalogue with photo- z and with assumed spectroscopic redshift, respectively.

We notice that the constraint precision of H_0 is quite low for TianQin. This is because the expected detection rate is relatively low, the detected events are not sufficient to suppress the random fluctuation, therefore the effect of spectroscopic redshift is not huge. However, for a network of detectors, one can expect more GW events, which make the uncertainty caused by the galaxy redshift measurement more dominant. We observe that the adoption of spectroscopic redshift can improve the precision of H_0 by a factor of 2. However, for the TianQin I+II+ET, the saturation described in Section IV C means a very precise estimate of H_0 can already been made even without the spectroscopic redshift. But still, by adopting the spectroscopic redshift, one can expect the H_0 to be constrained to a level better than 1%, using the weighted method.

B. Potential to address the Hubble tension

Astronomers are puzzled by the Hubble tension, which describes the inconsistency between the two typical Hubble constant measurement methods, reported as $74.03 \pm 1.42 \text{ km/s/Mpc}$ from Type Ia supernovae observations [7] (also see Ref. [9]) and $67.4 \pm 0.5 \text{ km/s/Mpc}$ from the *Planck* CMB measurements [3]. We notice that both methods are accompanied with remarkable accuracies, of about 1.9% and 0.7%, respectively. GW cosmology

TABLE II. Expected constraint precision of H_0 under six detector configures, assuming the survey galaxy catalogue with photo- z and with spectroscopic redshift. The error represents 68.27% confidence interval.

Network configuration	Constraint precision σ_{H_0}/H_0 (%)			
	Using photo- z catalogue		Using spectroscopic redshift catalogue	
	Fiducial method	Weighted method	Fiducial method	Weighted method
TianQin	$36.8^{+1.7}_{-1.8}$	$30.9^{+5.1}_{-5.1}$	$29.7^{+5.4}_{-6.2}$	$22.2^{+8.3}_{-9.8}$
TianQin I+II	$26.3^{+5.9}_{-6.9}$	$14.4^{+9.4}_{-7.6}$	$15.1^{+9.4}_{-6.9}$	$7.9^{+2.9}_{-3.2}$
TianQin+LISA	$25.2^{+6.4}_{-7.6}$	$11.6^{+8.2}_{-6.4}$	$12.4^{+6.2}_{-5.4}$	$6.4^{+1.6}_{-2.4}$
TianQin I+II+LISA	$12.2^{+5.3}_{-5.3}$	$4.1^{+0.8}_{-0.8}$	$5.7^{+1.5}_{-2.0}$	$3.3^{+0.7}_{-0.7}$
TianQin+ET	$4.67^{+1.80}_{-1.60}$	$1.51^{+0.13}_{-0.13}$	$2.10^{+0.25}_{-0.63}$	$1.32^{+0.10}_{-0.09}$
TianQin I+II+ET	$1.32^{+0.07}_{-0.09}$	$1.05^{+0.05}_{-0.06}$	$1.08^{+0.10}_{-0.09}$	$0.95^{+0.08}_{-0.08}$

with dark standard sirens provides an exciting new way of may clarifying or resolving the Hubble tension, as it is expected to be much less impacted by systematic errors. However, an equally accurate measurement would be required to achieve so. With the TianQin detectors, even in the most optimal scenario where we assume TianQin I+II with weighted method and a galaxy catalogue accompanied with spectroscopic redshift, the expected precision of H_0 can only reach 7.9%. When LISA is added, the precision can reach the level of 3.3%.

On the other hand, a multi-band GW detector network have a very prominent potential to estimate H_0 accurately. One can expect a H_0 precision of 1.51% and 1.05% for TianQin+ET and TianQin I+II+ET, respectively, which is very promising for helping to address, or at least shed light on the nature, for the Hubble tension.

C. P–P plot check

In order to alleviate the selection effect of the galaxies, we adopt a correction term in Eq. (12) in the hope to obtain an unbiased estimate of the Hubble constant. We would like to examine if the conclusion is indeed unbiased, for both the weighted method and the fiducial method. In order to do so, we perform a series of P–P plot as a consistency check as shown in FIG. 13. The horizontal axis shows the credible level, and the vertical axis showing the fraction of simulations that the true parameters locates within a certain credible interval. For a fully consistent method, we expect the P–P plot to be alongside the diagonal line, with some degree of random fluctuations. For more straightforward comparison, we perform Kolmogorov-Smirnov tests for different lines versus the diagonal line, and present the calculated p -value in TABLE III, with larger p -value represents a better consistency.

In the left panel, where we assume that only photo- z is available for the galaxies, most of the solid lines (or the fiducial method) deviate significantly from the diagonal, with a general pessimistic tendency. This is because the posterior probability of the cosmological parameters using the fiducial method does not gain sufficiently redshift information from a large number of candidate host galaxies, leading to a broad credible interval, while most likely the true value has already been enclosed. We observe, on the other hand, that the result from the weighted method (dashed lines) shows better consistency with the diagonal line, fluctuating well within the 3σ confidence interval, which indicates a successful implementation of an unbiased estimator for the Hubble constant.

If spectroscopic redshift are available for the galaxies, the P–P plots for both methods are statistically consistent with the diagonal for all configurations. This fact confirms the importance of an accurate measurement of galaxy redshifts on estimating the Hubble constant.

D. Effect of eccentricity on multi-band GW detection

In this work, we focus on GW sources with very small eccentricities ($e_0 = 0.01$ at 0.01Hz). For binary black holes evolved through isolated binary channel, this is a fair assumption, as the GW radiation is expected to circularise the orbit. However, if the SBBHs have a dynamical origin, they could retain larger eccentricities in the millihertz range [182, 183], which could affect the multi-band GW detection [184–186]. Indeed, the observations of GW190521 by LIGO and Virgo may suggest such possibility [22, 187, 188]. For extreme eccentricities the GW signals in the millihertz band could fall below the sensitivity of space-borne GW detectors [185]. Fortunately,

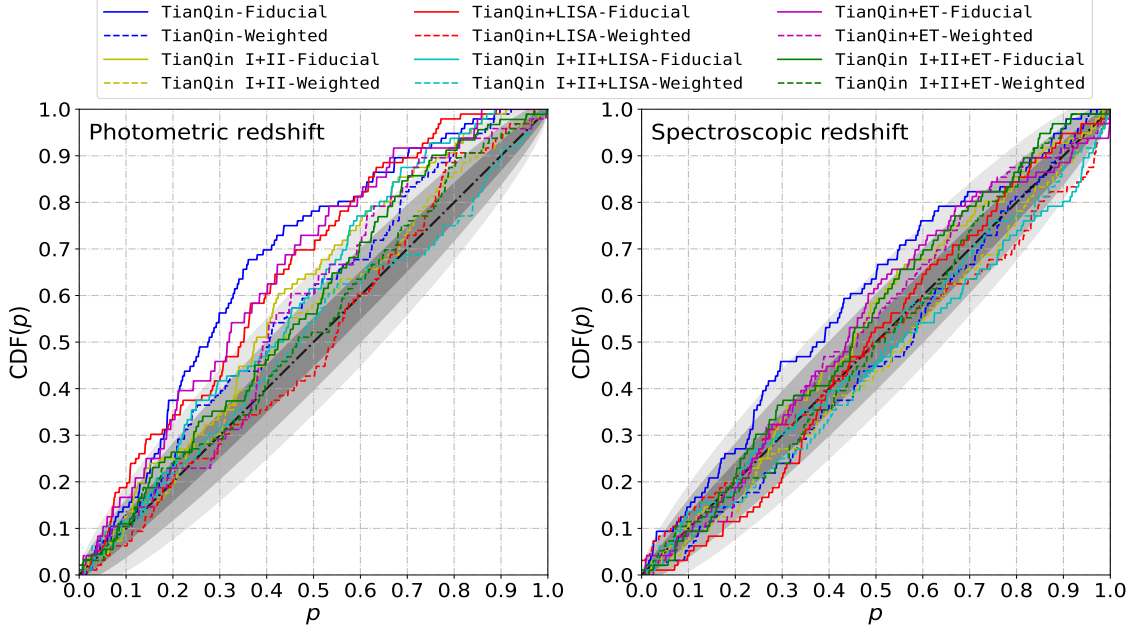


FIG. 13. P–P plot over 96 independent simulations on the Hubble constant estimation for various detector configurations. The p on the x axis is the credible level, and the $\text{CDF}(p)$ (cumulative distribution function, CDF) on the y axis is the fraction of simulations with true parameters within the credible interval. Results with different configurations are shown in different colors, with the fiducial method, the weighted method, and the diagonal line shown in solid, dashed, and dotted-dashed lines, respectively. Different gray shadows represent 1σ , 2σ , and 3σ confidence intervals, respectively. The left panel assumes photo- z for galaxies, while the right panel assumes that spectroscopic redshift are available.

TABLE III. The meta p -value of the distribution of H_0 estimations from multiple independent simulations under various detector configuration, relative to an expected uniform distribution over $[0, 1]$. The null hypothesis is setted so that the two distributions are consistent, therefore, a p -value less than 0.05 indicates that the simulation results deviate significantly from the ideal result.

Detector configuration	p -value			
	Using photo- z catalogue		Using spectroscopic redshift catalogue	
	Fiducial method	Weighted method	Fiducial method	Weighted method
TianQin	5.6×10^{-9}	0.0756	9.8×10^{-3}	0.3756
TianQin I+II	3.8×10^{-3}	0.2511	0.1774	0.5081
TianQin+LISA	2.3×10^{-5}	0.2513	0.2026	0.2419
TianQin I+II+LISA	1.9×10^{-3}	0.6767	0.1549	0.4871
TianQin+ET	2.6×10^{-3}	0.1085	0.1030	0.2690
TianQin I+II+ET	0.0209	0.4074	0.2386	0.5599

the majority of SBBHs are not expected to be associated with extreme eccentricities [162, 189], and the general conclusion of our study should not be overturn by the inclusion of eccentricities.

E. Other potential sources of constraint bias on the Hubble constant

There are many factors that can lead to bias in the estimation of the Hubble constant, here we list the potential sources of the bias involved in this work, as follows.

- The detectable SBBH sources are mainly distributed in $z \lesssim 0.2$, where the expansion of the universe can be approximated by Hubble's law. Therefore, in most cases, the model-dependent Ω_M do not affect our H_0 analysis results. However, a small number of GW events with $z \gtrsim 0.2$ show a certain constraint ability on Ω_M , such as the constraint results of TianQin+ET and TianQin I+II+ET. This means that the cosmological model will lead to a bias when using the SBBH events with higher redshifts to constrain H_0 with high precision.

- In the simulation of the GW event catalogue, the GW sources are randomly placed in one of galaxies in the survey galaxy catalogue. But in the actual H_0 estimation, the survey galaxy catalogue may not contain the true host galaxy of the GW source due to the selection effects like the Malmquist bias. The absence of the true redshift of the GW source in the statistical redshift could also lead to a bias on the estimation of H_0 .
- In the setup of the simulation, we take the median the photo- z estimate as the true cosmological redshift of the galaxy. However, the actual photo- z measurements have an intrinsic scatter and deviation relative to the spectroscopic redshifts [143, 146, 190, 191].
- If some of the SBBHs observed have an origin of primordial black holes [192–196], then the idea of host galaxy might no longer be meaningful. And conclusion drawn assuming all SBBHs are astronomically originated might be misleading.

Of course, there are method to alleviate the bias. For example, the bias of H_0 caused by cosmological model can be avoided by fitting model-independent high-order expansion of the ‘ $D_L - z$ relation’ [197, 198], or using model-independent parameter estimation method such as Gaussian processes [60, 64, 199]. The selection effect in the galaxy survey catalogue can be corrected by follow-up deeper field galaxy survey triggered by the GW detection [200–202], utilising both ground-based telescopes [203, 204] and space telescope [169, 180]. The bias introduced from photo- z can be eliminated by follow-up spectroscopic measurement. The possible contamination from primordial black holes require further investigation, but internal consistency check as introduced in [84, 90] may help identify and remove anomaly.

VI. CONCLUSIONS AND OUTLOOK

In this work we investigate the potential of the space-borne GW detectors that using SBBH GW events (assuming the ‘Power Law + Peak’ model) as dark standard sirens to constrain the Hubble constant. Several different detection scenarios are considered, e.g., single detector(s), such as TianQin and TianQin I+II; multiple detectors network, such as TianQin+LISA and TianQin I+II+LISA; and multi-band GW detector network, such as TianQin+ET and TianQin I+II+ET. The redshift information is obtained statistically from the photometric survey galaxy catalogue by matching the sky localization and possible redshift range of the SBBH sources with the position and redshift of galaxies (we adopt the GWENS catalogue in this work). Two methods are used to assign the weight of galaxies, including the fiducial method, in which each galaxy within the error box has uniform weight, and the weighted method, in which the weight of a galaxy is proportional to the galaxy mass derived from the luminosity through the **Le Phare** method.

Compared with single detector detection, both multi-detector network and multi-band GW observation can significantly improve the detection rate and spatial localizations. The weighted method can significantly improve the constraint precision of the Hubble constant in comparison with the fiducial method. Using the fiducial method and the weighted method, in TianQin-alone scenario, the constraint precision of H_0 is expected to be only about 36.8% and about 30.9%, respectively; in TianQin I+II detection scenario, the precision of H_0 is expected to be about 26.3% and about 14.4%, respectively. In the TianQin+LISA and TianQin I+II+LISA detection scenarios, the constraint precision of H_0 are expected to be about 11.6% and about 4.1% using the weighted method, respectively. In the multi-band GW detection scenarios, the precision of H_0 constrain by using the weighted method can reach about 1.5% and 1.1% under TianQin+ET configuration and TianQin I+II+ET configuration, respectively. It should be emphasized that the weighted method and the multi-band GW detection both have particularly significant improvements to the constraint of H_0 .

Apart from H_0 , the space-borne GW detector can hardly constrain any other cosmological parameter, such as Ω_M , through the detections of SBBH inspiral GW signals. However, constraining other cosmological parameters is possible with other types of GW sources like MBHB mergers [84, 85, 90]. The MBHB sources generally have very high SNRs, and the event horizons can reach high redshifts ($z \gg 1$). Therefore, a combination of SBBH and MBHB GW observation can achieve a more comprehensive GW cosmology study.

In addition, we study how much the spectroscopic redshift information improves the constraining power on the Hubble constant, which not only increases the precision of the Hubble constant, but also improves the accuracy of the constraint. And finally, we also tested the reliability of our Bayesian analysis framework and weighting method of galaxies by performing a consistency test through the P–P plot method.

Some issues are still open for future studies, to make the overall study more realistic, like introducing a full frequency response [136] or the time-delay interferometry (TDI) response [205]. Instead of the FIM method, one can also use MCMC to obtain more realistic GW parameter estimations [206]. The calibration uncertainty of the laser interferometer of the ground-based GW detector can lead to systematic errors in the luminosity distance measurement [207–209], such as for ET. We leave such issues for future investigations.

ACKNOWLEDGEMENTS

This work has been supported by the Guangdong Major Project of Basic and Applied Basic Research (Grant No. 2019B030302001), the Natural Science Foundation of China (Grants No. 12173104, 11805286, and 11690022), and National Key Research and Development Program of China (No. 2020YFC2201400). We acknowledge the use of the *Kunlun* cluster, a supercomputer owned by the School of Physics and Astronomy, Sun Yat-Sen University, and of the *Tianhe-2*, a supercomputer owned by the National Supercomputing Center in GuangZhou. The authors acknowledge the uses of the calculating utilities of *emcee* [170, 171], *numpy* [210], *scipy* [211], and *LALSuite* [212], and the plotting utilities of *matplotlib* [213], and *corner* [214]. The authors also thank Xiao-Dong Li and Martin Hendry for helpful discussions.

-
- [1] B. F. Schutz. Determining the Hubble constant from gravitational wave observations. *Nature*, 323(6086):310–311, September 1986.
 - [2] P. A. R. Ade et al. Planck 2015 results. XIII. Cosmological parameters. *Astron. Astrophys.*, 594:A13, 2016.
 - [3] N. Aghanim et al. Planck 2018 results. VI. Cosmological parameters. *Astron. Astrophys.*, 641:A6, 2020. [Erratum: *Astron. Astrophys.* 652, C4 (2021)].
 - [4] Wendy L. Freedman. Cosmology at a Crossroads. *Nature Astron.*, 1:0121, 2017.
 - [5] Wendy L. Freedman, Barry F. Madore, Dylan Hatt, Taylor J. Hoyt, In Sung Jang, Rachael L. Beaton, Christopher R. Burns, Myung Gyoon Lee, Andrew J. Monson, Jillian R. Neeley, M. M. Phillips, Jeffrey A. Rich, and Mark Seibert. The carnegie-chicago hubble program. VIII. an independent determination of the hubble constant based on the tip of the red giant branch. *The Astrophysical Journal*, 882(1):34, aug 2019.
 - [6] Wendy L. Freedman. Measurements of the Hubble Constant: Tensions in Perspective. 6 2021.
 - [7] Adam G. Riess, Stefano Casertano, Wenlong Yuan, Lucas M. Macri, and Dan Scolnic. Large Magellanic Cloud Cepheid Standards Provide a 1% Foundation for the Determination of the Hubble Constant and Stronger Evidence for Physics beyond Λ CDM. *Astrophys. J.*, 876(1):85, 2019.
 - [8] Adam G. Riess. The Expansion of the Universe is Faster than Expected. *Nature Rev. Phys.*, 2(1):10–12, 2019.
 - [9] Adam G. Riess, Stefano Casertano, Wenlong Yuan, J. Bradley Bowers, Lucas Macri, Joel C. Zinn, and Dan Scolnic. Cosmic Distances Calibrated to 1% Precision with Gaia EDR3 Parallaxes and Hubble Space Telescope Photometry of 75 Milky Way Cepheids Confirm Tension with Λ CDM. *Astrophys. J. Lett.*, 908(1):L6, 2021.
 - [10] Hsin-Yu Chen, Maya Fishbach, and Daniel E. Holz. A two per cent Hubble constant measurement from standard sirens within five years. *Nature*, 562(7728):545–547, 2018.
 - [11] Stephen M. Feeney, Hiranya V. Peiris, Andrew R. Williamson, Samaya M. Nissanke, Daniel J. Mortlock, Justin Alsing, and Dan Scolnic. Prospects for resolving the Hubble constant tension with standard sirens. *Phys. Rev. Lett.*, 122(6):061105, 2019.
 - [12] Ssohrab Borhanian, Arnab Dhani, Anuradha Gupta, K. G. Arun, and B. S. Sathyaprakash. Dark Sirens to Resolve the Hubble–Lemaître Tension. *Astrophys. J. Lett.*, 905(2):L28, 2020.
 - [13] B. P. Abbott, R. Abbott, T. D. Abbott, M. R. Abernathy, F. Acernese, K. Ackley, C. Adams, T. Adams, P. Addesso, R. X. Adhikari, and et al. Observation of Gravitational Waves from a Binary Black Hole Merger. *Phys. Rev. Lett.*, 116(6):061102, February 2016.
 - [14] B. P. Abbott, R. Abbott, T. D. Abbott, M. R. Abernathy, F. Acernese, K. Ackley, C. Adams, T. Adams, P. Addesso, R. X. Adhikari, and et al. GW151226: Observation of Gravitational Waves from a 22-Solar-Mass Binary Black Hole Coalescence. *Phys. Rev. Lett.*, 116(24):241103, June 2016.
 - [15] B. P. Abbott, R. Abbott, T. D. Abbott, F. Acernese, K. Ackley, C. Adams, T. Adams, P. Addesso, R. X. Adhikari, V. B. Adya, and et al. GW170104: Observation of a 50-Solar-Mass Binary Black Hole Coalescence at Redshift 0.2. *Phys. Rev. Lett.*, 118(22):221101, June 2017.
 - [16] B. P. Abbott, R. Abbott, T. D. Abbott, F. Acernese, K. Ackley, C. Adams, T. Adams, P. Addesso, R. X. Adhikari, V. B. Adya, and et al. GW170608: Observation of a 19 Solar-mass Binary Black Hole Coalescence. *ApJ*, 851(2):L35, December 2017.
 - [17] B. P. Abbott, R. Abbott, T. D. Abbott, F. Acernese, K. Ackley, C. Adams, T. Adams, P. Addesso, R. X. Adhikari, V. B. Adya, and et al. GW170814: A Three-Detector Observation of Gravitational Waves from a Binary Black Hole Coalescence. *Phys. Rev. Lett.*, 119(14):141101, October 2017.
 - [18] B. P. Abbott, R. Abbott, T. D. Abbott, F. Acernese, K. Ackley, C. Adams, T. Adams, P. Addesso, R. X. Adhikari, V. B. Adya, and et al. GW170817: Observation of Gravitational Waves from a Binary Neutron Star Inspiral. *Phys. Rev. Lett.*, 119(16):161101, October 2017.
 - [19] B.P. Abbott et al. GWTC-1: A Gravitational-Wave Transient Catalog of Compact Binary Mergers Observed by LIGO and Virgo during the First and Second Observing Runs. *Phys. Rev. X*, 9(3):031040, 2019.
 - [20] R. Abbott et al. GW190412: Observation of a Binary-Black-Hole Coalescence with Asymmetric Masses. *Phys. Rev. D*, 102(4):043015, 2020.
 - [21] B. P. Abbott et al. GW190425: Observation of a Compact Binary Coalescence with Total Mass $\sim 3.4M_{\odot}$. *Astrophys. J. Lett.*, 892(1):L3, 2020.
 - [22] R. Abbott et al. GW190521: A Binary Black Hole Merger with a Total Mass of $150M_{\odot}$. *Phys. Rev. Lett.*, 125(10):101102, 2020.

- [23] R. Abbott et al. GW190814: Gravitational Waves from the Coalescence of a 23 Solar Mass Black Hole with a 2.6 Solar Mass Compact Object. *Astrophys. J. Lett.*, 896(2):L44, 2020.
- [24] R. Abbott et al. GWTC-2: Compact Binary Coalescences Observed by LIGO and Virgo During the First Half of the Third Observing Run. 10 2020.
- [25] R. Abbott et al. GWTC-2.1: Deep Extended Catalog of Compact Binary Coalescences Observed by LIGO and Virgo During the First Half of the Third Observing Run. 8 2021.
- [26] R. Abbott et al. Observation of Gravitational Waves from Two Neutron Star–Black Hole Coalescences. *Astrophys. J. Lett.*, 915(1):L5, 2021.
- [27] T. Akutsu et al. KAGRA: 2.5 Generation Interferometric Gravitational Wave Detector. *Nature Astron.*, 3(1):35–40, 2019.
- [28] C. S. Unnikrishnan. IndIGO and LIGO-India: Scope and plans for gravitational wave research and precision metrology in India. *Int. J. Mod. Phys. D*, 22:1341010, 2013.
- [29] Samaya Nissanke, Daniel E. Holz, Neal Dalal, Scott A. Hughes, Jonathan L. Sievers, and Christopher M. Hirata. Determining the Hubble constant from gravitational wave observations of merging compact binaries. 7 2013.
- [30] Salvatore Vitale and Hsin-Yu Chen. Measuring the Hubble constant with neutron star black hole mergers. *Phys. Rev. Lett.*, 121(2):021303, 2018.
- [31] Daniel J. Mortlock, Stephen M. Feeney, Hiranya V. Peiris, Andrew R. Williamson, and Samaya M. Nissanke. Unbiased Hubble constant estimation from binary neutron star mergers. *Phys. Rev. D*, 100(10):103523, 2019.
- [32] B.P. Abbott et al. Gravitational Waves and Gamma-rays from a Binary Neutron Star Merger: GW170817 and GRB 170817A. *Astrophys. J. Lett.*, 848(2):L13, 2017.
- [33] M. Soares-Santos et al. The Electromagnetic Counterpart of the Binary Neutron Star Merger LIGO/Virgo GW170817. I. Discovery of the Optical Counterpart Using the Dark Energy Camera. *Astrophys. J. Lett.*, 848(2):L16, 2017.
- [34] B. P. Abbott et al. Multi-messenger Observations of a Binary Neutron Star Merger. *Astrophys. J. Lett.*, 848(2):L12, 2017.
- [35] B. P. Abbott et al. A gravitational-wave standard siren measurement of the Hubble constant. *Nature*, 551(7678):85–88, 2017.
- [36] M. Fishbach et al. A Standard Siren Measurement of the Hubble Constant from GW170817 without the Electromagnetic Counterpart. *Astrophys. J. Lett.*, 871(1):L13, 2019.
- [37] C. Guidorzi et al. Improved Constraints on H_0 from a Combined Analysis of Gravitational-wave and Electromagnetic Emission from GW170817. *Astrophys. J. Lett.*, 851(2):L36, 2017.
- [38] Kenta Hotokezaka, Ehud Nakar, Ore Gottlieb, Samaya Nissanke, Kento Masuda, Gregg Hallinan, Kunal P. Mooley, and Adam. T. Deller. A Hubble constant measurement from superluminal motion of the jet in GW170817. *Nature Astron.*, 3(10):940–944, 2019.
- [39] B. McKernan, K. E. S. Ford, I. Bartos, M. J. Graham, W. Lyra, S. Marka, Z. Marka, N. P. Ross, D. Stern, and Y. Yang. Ram-pressure stripping of a kicked Hill sphere: Prompt electromagnetic emission from the merger of stellar mass black holes in an AGN accretion disk. *Astrophys. J. Lett.*, 884(2):L50, 2019.
- [40] M. J. Graham et al. Candidate Electromagnetic Counterpart to the Binary Black Hole Merger Gravitational Wave Event S190521g. *Phys. Rev. Lett.*, 124(25):251102, 2020.
- [41] M. Soares-Santos et al. First Measurement of the Hubble Constant from a Dark Standard Siren using the Dark Energy Survey Galaxies and the LIGO/Virgo Binary–Black-hole Merger GW170814. *Astrophys. J. Lett.*, 876(1):L7, 2019.
- [42] A. Palmese et al. A statistical standard siren measurement of the Hubble constant from the LIGO/Virgo gravitational wave compact object merger GW190814 and Dark Energy Survey galaxies. *Astrophys. J. Lett.*, 900(2):L33, 2020.
- [43] Sergiy Vasylyev and Alex Filippenko. A Measurement of the Hubble Constant using Gravitational Waves from the Binary Merger GW190814. *Astrophys. J.*, 902(2):149, 2020.
- [44] B. P. Abbott et al. A Gravitational-wave Measurement of the Hubble Constant Following the Second Observing Run of Advanced LIGO and Virgo. *Astrophys. J.*, 909(2):218, 2021.
- [45] Walter Del Pozzo. Inference of the cosmological parameters from gravitational waves: application to second generation interferometers. *Phys. Rev. D*, 86:043011, 2012.
- [46] Stephen R. Taylor, Jonathan R. Gair, and Ilya Mandel. Hubble without the Hubble: Cosmology using advanced gravitational-wave detectors alone. *Phys. Rev. D*, 85:023535, 2012.
- [47] Remya Nair, Sukanta Bose, and Tarun Deep Saini. Measuring the Hubble constant: Gravitational wave observations meet galaxy clustering. *Phys. Rev. D*, 98(2):023502, 2018.
- [48] Will M. Farr, Maya Fishbach, Jiani Ye, and Daniel Holz. A Future Percent-Level Measurement of the Hubble Expansion at Redshift 0.8 With Advanced LIGO. *Astrophys. J. Lett.*, 883(2):L42, 2019.
- [49] Rachel Gray et al. Cosmological inference using gravitational wave standard sirens: A mock data analysis. *Phys. Rev. D*, 101(12):122001, 2020.
- [50] Sayantani Bera, Divya Rana, Surhud More, and Sukanta Bose. Incompleteness Matters Not: Inference of H_0 from Binary Black Hole–Galaxy Cross-correlations. *Astrophys. J.*, 902(1):79, 2020.
- [51] Andreas Finke, Stefano Foffa, Francesco Iacovelli, Michele Maggiore, and Michele Mancarella. Cosmology with LIGO/Virgo dark sirens: Hubble parameter and modified gravitational wave propagation. 1 2021.
- [52] M. Punturo et al. The Einstein Telescope: A third-generation gravitational wave observatory. *Class. Quant. Grav.*, 27:194002, 2010.
- [53] B. Sathyaprakash et al. Scientific Objectives of Einstein Telescope. *Class. Quant. Grav.*, 29:124013, 2012. [Erratum: *Class.Quant.Grav.* 30, 079501 (2013)].

- [54] Michele Maggiore et al. Science Case for the Einstein Telescope. *JCAP*, 03:050, 2020.
- [55] Sheila Dwyer, Daniel Sigg, Stefan W. Ballmer, Lisa Barsotti, Nergis Mavalvala, and Matthew Evans. Gravitational wave detector with cosmological reach. *Phys. Rev. D*, 91(8):082001, 2015.
- [56] Benjamin P Abbott et al. Exploring the Sensitivity of Next Generation Gravitational Wave Detectors. *Class. Quant. Grav.*, 34(4):044001, 2017.
- [57] W. Zhao, C. Van Den Broeck, D. Baskaran, and T. G. F. Li. Determination of Dark Energy by the Einstein Telescope: Comparing with CMB, BAO and SNIa Observations. *Phys. Rev. D*, 83:023005, 2011.
- [58] Wen Zhao and Linqing Wen. Localization accuracy of compact binary coalescences detected by the third-generation gravitational-wave detectors and implication for cosmology. *Phys. Rev. D*, 97(6):064031, 2018.
- [59] Stephen R. Taylor and Jonathan R. Gair. Cosmology with the lights off: standard sirens in the Einstein Telescope era. *Phys. Rev. D*, 86:023502, 2012.
- [60] Marina Seikel, Chris Clarkson, and Mathew Smith. Reconstruction of dark energy and expansion dynamics using Gaussian processes. *JCAP*, 06:036, 2012.
- [61] C. Messenger and J. Read. Measuring a cosmological distance-redshift relationship using only gravitational wave observations of binary neutron star coalescences. *Phys. Rev. Lett.*, 108:091101, 2012.
- [62] C. Messenger, Kentaro Takami, Sarah Gossan, Luciano Rezzolla, and B. S. Sathyaprakash. Source Redshifts from Gravitational-Wave Observations of Binary Neutron Star Mergers. *Phys. Rev. X*, 4(4):041004, 2014.
- [63] Walter Del Pozzo, Tjonnie G. F. Li, and Chris Messenger. Cosmological inference using only gravitational wave observations of binary neutron stars. *Phys. Rev. D*, 95(4):043502, 2017.
- [64] Rong-Gen Cai and Tao Yang. Estimating cosmological parameters by the simulated data of gravitational waves from the Einstein Telescope. *Phys. Rev. D*, 95(4):044024, 2017.
- [65] Minghui Du, Weiqiang Yang, Lixin Xu, Supriya Pan, and David F. Mota. Future constraints on dynamical dark-energy using gravitational-wave standard sirens. *Phys. Rev. D*, 100(4):043535, 2019.
- [66] Xuan-Neng Zhang, Ling-Feng Wang, Jing-Fei Zhang, and Xin Zhang. Improving cosmological parameter estimation with the future gravitational-wave standard siren observation from the Einstein Telescope. *Phys. Rev. D*, 99(6):063510, 2019.
- [67] Josiel Mendonça Soares de Souza and Riccardo Sturani. Cosmological model selection from standard siren detections by third-generation gravitational wave observatories. *Phys. Dark Univ.*, 32:100830, 2021.
- [68] Jing-Fei Zhang, Ming Zhang, Shang-Jie Jin, Jing-Zhao Qi, and Xin Zhang. Cosmological parameter estimation with future gravitational wave standard siren observation from the Einstein Telescope. *JCAP*, 09:068, 2019.
- [69] Jiming Yu, Yu Wang, Wen Zhao, and Youjun Lu. Hunting for the host galaxy groups of binary black holes and the application in constraining Hubble constant. *Mon. Not. Roy. Astron. Soc.*, 498(2):1786–1800, 2020.
- [70] Zhi-Qiang You, Xing-Jiang Zhu, Gregory Ashton, Eric Thrane, and Zong-Hong Zhu. Standard-siren cosmology using gravitational waves from binary black holes. *Astrophys. J.*, 908(2):215, 2021.
- [71] Alexander Bonilla, Suresh Kumar, Rafael C. Nunes, and Supriya Pan. Reconstruction of the dark sectors’ interaction: A model-independent inference and forecast from GW standard sirens. 2 2021.
- [72] Jun Luo et al. TianQin: a space-borne gravitational wave detector. *Class. Quant. Grav.*, 33(3):035010, 2016.
- [73] Pau Amaro-Seoane et al. Laser Interferometer Space Antenna. 2 2017.
- [74] Antoine Klein et al. Science with the space-based interferometer eLISA: Supermassive black hole binaries. *Phys. Rev. D*, 93(2):024003, 2016.
- [75] Enrico Barausse, Irina Dvorkin, Michael Tremmel, Marta Volonteri, and Matteo Bonetti. Massive Black Hole Merger Rates: The Effect of Kiloparsec Separation Wandering and Supernova Feedback. *Astrophys. J.*, 904(1):16, 2020.
- [76] Hai-Tian Wang, Zhen Jiang, Alberto Sesana, Enrico Barausse, Shun-Jia Huang, Yi-Fan Wang, Wen-Fan Feng, Yan Wang, Yi-Ming Hu, Jianwei Mei, and Jun Luo. Science with the TianQin observatory: Preliminary results on massive black hole binaries. *Phys. Rev. D*, 100(4):043003, August 2019.
- [77] Stanislav Babak, Jonathan Gair, Alberto Sesana, Enrico Barausse, Carlos F. Sopuerta, Christopher P. L. Berry, Emanuele Berti, Pau Amaro-Seoane, Antoine Petiteau, and Antoine Klein. Science with the space-based interferometer LISA. V: Extreme mass-ratio inspirals. *Phys. Rev. D*, 95(10):103012, 2017.
- [78] Jonathan R. Gair, Stanislav Babak, Alberto Sesana, Pau Amaro-Seoane, Enrico Barausse, Christopher P. L. Berry, Emanuele Berti, and Carlos Sopuerta. Prospects for observing extreme-mass-ratio inspirals with LISA. *J. Phys. Conf. Ser.*, 840(1):012021, 2017.
- [79] Hui-Min Fan, Yi-Ming Hu, Enrico Barausse, Alberto Sesana, Jian-dong Zhang, Xuefeng Zhang, Tie-Guang Zi, and Jianwei Mei. Science with the TianQin observatory: Preliminary result on extreme-mass-ratio inspirals. *Phys. Rev. D*, 102(6):063016, 2020.
- [80] Koutarou Kyutoku and Naoki Seto. Concise estimate of the expected number of detections for stellar-mass binary black holes by eLISA. *Mon. Not. Roy. Astron. Soc.*, 462(2):2177–2183, 2016.
- [81] Shuai Liu, Yi-Ming Hu, Jian-dong Zhang, and Jianwei Mei. Science with the TianQin observatory: Preliminary results on stellar-mass binary black holes. *Phys. Rev. D*, 101(10):103027, 2020.
- [82] Daniel E. Holz and Scott A. Hughes. Using gravitational-wave standard sirens. *Astrophys. J.*, 629:15–22, 2005.
- [83] Stanislav Babak, Jonathan R. Gair, Antoine Petiteau, and Alberto Sesana. Fundamental physics and cosmology with LISA. *Class. Quant. Grav.*, 28:114001, 2011.
- [84] Antoine Petiteau, Stanislav Babak, and Alberto Sesana. Constraining the dark energy equation of state using LISA observations of spinning Massive Black Hole binaries. *Astrophys. J.*, 732:82, 2011.
- [85] Nicola Tamanini, Chiara Caprini, Enrico Barausse, Alberto Sesana, Antoine Klein, and Antoine Petiteau. Science with the space-based interferometer eLISA. III: Probing the expansion of the Universe using gravitational wave standard sirens. *JCAP*, 04:002, 2016.

- [86] Chiara Caprini and Nicola Tamanini. Constraining early and interacting dark energy with gravitational wave standard sirens: the potential of the eLISA mission. *JCAP*, 10:006, 2016.
- [87] Rong-Gen Cai, Nicola Tamanini, and Tao Yang. Reconstructing the dark sector interaction with LISA. *JCAP*, 05:031, 2017.
- [88] Ling-Feng Wang, Ze-Wei Zhao, Jing-Fei Zhang, and Xin Zhang. A preliminary forecast for cosmological parameter estimation with gravitational-wave standard sirens from TianQin. *JCAP*, 11:012, 2020.
- [89] Renjie Wang, Wen-Hong Ruan, Qing Yang, Zong-Kuan Guo, Rong-Gen Cai, and Bin Hu. Hubble parameter estimation via dark sirens with the LISA-Taiji network. 10 2020.
- [90] Liang-Gui Zhu, Yi-Ming Hu, Hai-Tian Wang, Jian-Dong Zhang, Xiao-Dong Li, Martin Hendry, and Jianwei Mei. Constraining the cosmological parameters using gravitational wave observations of massive black hole binaries and statistical redshift information. 4 2021.
- [91] Chelsea L. MacLeod and Craig J. Hogan. Precision of Hubble constant derived using black hole binary absolute distances and statistical redshift information. *Phys. Rev. D*, 77:043512, 2008.
- [92] Danny Laghi, Nicola Tamanini, Walter Del Pozzo, Alberto Sesana, Jonathan Gair, and Stanislav Babak. Gravitational wave cosmology with extreme mass-ratio inspirals. 2 2021.
- [93] Koutarou Kyutoku and Naoki Seto. Gravitational-wave cosmography with LISA and the Hubble tension. *Phys. Rev. D*, 95(8):083525, 2017.
- [94] Walter Del Pozzo, Alberto Sesana, and Antoine Klein. Stellar binary black holes in the LISA band: a new class of standard sirens. *Mon. Not. Roy. Astron. Soc.*, 475(3):3485–3492, 2018.
- [95] Alberto Sesana. Prospects for Multiband Gravitational-Wave Astronomy after GW150914. *Phys. Rev. Lett.*, 116(23):231102, 2016.
- [96] Alberto Sesana. Multi-band gravitational wave astronomy: science with joint space- and ground-based observations of black hole binaries. *J. Phys. Conf. Ser.*, 840(1):012018, 2017.
- [97] Salvatore Vitale. Multiband Gravitational-Wave Astronomy: Parameter Estimation and Tests of General Relativity with Space- and Ground-Based Detectors. *Phys. Rev. Lett.*, 117(5):051102, 2016.
- [98] Christopher J. Moore, Davide Gerosa, and Antoine Klein. Are stellar-mass black-hole binaries too quiet for LISA? *Mon. Not. Roy. Astron. Soc.*, 488(1):L94–L98, 2019.
- [99] Becca Ewing, Surabhi Sachdev, Ssohrab Borhanian, and B. S. Sathyaprakash. Archival searches for stellar-mass binary black holes in LISA data. *Phys. Rev. D*, 103(2):023025, 2021.
- [100] Stefan Grimm and Jan Harms. Multiband gravitational-wave parameter estimation: A study of future detectors. *Phys. Rev. D*, 102(2):022007, 2020.
- [101] Enrico Barausse, Nicolás Yunes, and Katie Chamberlain. Theory-Agnostic Constraints on Black-Hole Dipole Radiation with Multiband Gravitational-Wave Astrophysics. *Phys. Rev. Lett.*, 116(24):241104, 2016.
- [102] Kaze W. K. Wong, Ely D. Kovetz, Curt Cutler, and Emanuele Berti. Expanding the LISA Horizon from the Ground. *Phys. Rev. Lett.*, 121(25):251102, 2018.
- [103] Davide Gerosa, Sizheng Ma, Kaze W. K. Wong, Emanuele Berti, Richard O’Shaughnessy, Yanbei Chen, and Krzysztof Belczynski. Multiband gravitational-wave event rates and stellar physics. *Phys. Rev. D*, 99(10):103004, 2019.
- [104] Curt Cutler et al. What we can learn from multi-band observations of black hole binaries. 3 2019.
- [105] Chang Liu, Lijing Shao, Junjie Zhao, and Yong Gao. Multiband Observation of LIGO/Virgo Binary Black Hole Mergers in the Gravitational-wave Transient Catalog GWTC-1. *Mon. Not. Roy. Astron. Soc.*, 496(1):182–196, 2020.
- [106] Niccolò Muttoni, Alberto Mangiagli, Alberto Sesana, Danny Laghi, Walter Del Pozzo, and David Izquierdo-Villalba. Multi-band gravitational wave cosmology with stellar origin black hole binaries. 9 2021.
- [107] Jun Luo et al. The first round result from the TianQin-1 satellite. *Class. Quant. Grav.*, 37(18):185013, 2020.
- [108] Jianwei Mei et al. The TianQin project: current progress on science and technology. 8 2020.
- [109] Monica Colpi and Alberto Sesana. *Gravitational Wave Sources in the Era of Multi-Band Gravitational Wave Astronomy*, pages 43–140. 2017.
- [110] Wen Zhao. Gravitational-wave standard siren and cosmology. *Scientia Sinica Physica, Mechanica & Astronomica*, 48(7):079805, July 2018.
- [111] Samaya Nissanke, Daniel E. Holz, Scott A. Hughes, Neal Dalal, and Jonathan L. Sievers. Exploring short gamma-ray bursts as gravitational-wave standard sirens. *Astrophys. J.*, 725:496–514, 2010.
- [112] P. K. Blanchard et al. The Electromagnetic Counterpart of the Binary Neutron Star Merger LIGO/VIRGO GW170817. VII. Properties of the Host Galaxy and Constraints on the Merger Timescale. *Astrophys. J. Lett.*, 848(2):L22, 2017.
- [113] Li-Xin Li and Bohdan Paczynski. Transient events from neutron star mergers. *Astrophys. J. Lett.*, 507:L59, 1998.
- [114] B. D. Metzger, G. Martínez-Pinedo, S. Darbha, E. Quataert, A. Arcones, D. Kasen, R. Thomas, P. Nugent, I. V. Panov, and N. T. Zinner. Electromagnetic counterparts of compact object mergers powered by the radioactive decay of r-process nuclei. *MNRAS*, 406(4):2650–2662, August 2010.
- [115] N. R. Tanvir et al. The Emergence of a Lanthanide-Rich Kilonova Following the Merger of Two Neutron Stars. *Astrophys. J. Lett.*, 848(2):L27, 2017.
- [116] Bülent Kiziltan, Athanasios Kottas, Maria De Yoreo, and Stephen E. Thorsett. The Neutron Star Mass Distribution. *Astrophys. J.*, 778:66, 2013.
- [117] Masamune Oguri. Measuring the distance-redshift relation with the cross-correlation of gravitational wave standard sirens and galaxies. *Phys. Rev. D*, 93(8):083511, 2016.
- [118] Pengjie Zhang. Accurate redshift determination of standard sirens by the luminosity distance space-redshift space large scale structure cross correlation. 11 2018.

- [119] Suvodip Mukherjee, Benjamin D. Wandelt, Samaya M. Nissanke, and Alessandra Silvestri. Accurate precision Cosmology with redshift unknown gravitational wave sources. *Phys. Rev. D*, 103(4):043520, 2021.
- [120] Cristina Cigarán Díaz and Suvodip Mukherjee. Mapping the cosmic expansion history from LIGO-Virgo-KAGRA in synergy with DESI and SPHEREx. 7 2021.
- [121] Xuheng Ding, Marek Biesiada, Xiaogang Zheng, Kai Liao, Zhengxiang Li, and Zong-Hong Zhu. Cosmological inference from standard sirens without redshift measurements. *JCAP*, 04:033, 2019.
- [122] Hebertt Leandro, Valerio Marra, and Riccardo Sturani. Measuring the Hubble constant with black sirens. 9 2021.
- [123] Naoki Seto, Seiji Kawamura, and Takashi Nakamura. Possibility of direct measurement of the acceleration of the universe using 0.1-Hz band laser interferometer gravitational wave antenna in space. *Phys. Rev. Lett.*, 87:221103, 2001.
- [124] Atsushi Nishizawa, Atsushi Taruya, and Shun Saito. Tracing the redshift evolution of Hubble parameter with gravitational-wave standard sirens. *Phys. Rev. D*, 83:084045, 2011.
- [125] Atsushi Nishizawa, Kent Yagi, Atsushi Taruya, and Takahiro Tanaka. Cosmology with space-based gravitational-wave detectors — dark energy and primordial gravitational waves —. *Phys. Rev. D*, 85:044047, 2012.
- [126] Ilya Mandel, Will M. Farr, and Jonathan R. Gair. Extracting distribution parameters from multiple uncertain observations with selection biases. *Mon. Not. Roy. Astron. Soc.*, 486(1):1086–1093, 2019.
- [127] Lee S. Finn. Detection, measurement, and gravitational radiation. *Phys. Rev. D*, 46:5236–5249, Dec 1992.
- [128] Gergely Dálya, Gábor Galgóczi, László Dobos, Zsolt Frei, Ik Siong Heng, Ronaldas Macas, Christopher Messenger, Péter Raffai, and Rafael S. de Souza. GLADE: A galaxy catalogue for multimessenger searches in the advanced gravitational-wave detector era. *Mon. Not. Roy. Astron. Soc.*, 479(2):2374–2381, 2018.
- [129] Kip S. Thorne. In S. W. Hawking and W. Israel, editors, *Three hundred years of gravitation*, pages 330–458. Cambridge University Press, Cambridge, England, 1987.
- [130] A. Freise, S. Chelkowski, S. Hild, W. Del Pozzo, A. Perreca, and A. Vecchio. Triple Michelson Interferometer for a Third-Generation Gravitational Wave Detector. *Class. Quant. Grav.*, 26:085012, 2009.
- [131] Xin-Chun Hu, Xiao-Hong Li, Yan Wang, Wen-Fan Feng, Ming-Yue Zhou, Yi-Ming Hu, Shou-Cun Hu, Jian-Wei Mei, and Cheng-Gang Shao. Fundamentals of the orbit and response for TianQin. *Class. Quant. Grav.*, 35(9):095008, 2018.
- [132] Curt Cutler. Angular resolution of the LISA gravitational wave detector. *Phys. Rev. D*, 57:7089–7102, 1998.
- [133] Neil J. Cornish and Louis J. Rubbo. The LISA response function. *Phys. Rev. D*, 67:022001, 2003. [Erratum: *Phys.Rev.D* 67, 029905 (2003)].
- [134] Piotr Jaranowski, Andrzej Krolak, and Bernard F. Schutz. Data analysis of gravitational - wave signals from spinning neutron stars. 1. The Signal and its detection. *Phys. Rev. D*, 58:063001, 1998.
- [135] Travis Robson, Neil J. Cornish, and Chang Liu. The construction and use of LISA sensitivity curves. *Classical and Quantum Gravity*, 36(10):105011, May 2019.
- [136] Chunyu Zhang, Qing Gao, Yungui Gong, Bin Wang, Alan J. Weinstein, and Chao Zhang. Full analytical formulas for frequency response of space-based gravitational wave detectors. *Phys. Rev. D*, 101(12):124027, 2020.
- [137] Curt Cutler and Eanna E. Flanagan. Gravitational waves from merging compact binaries: How accurately can one extract the binary’s parameters from the inspiral wave form? *Phys. Rev. D*, 49:2658–2697, 1994.
- [138] S. Hild et al. Sensitivity Studies for Third-Generation Gravitational Wave Observatories. *Class. Quant. Grav.*, 28:094013, 2011.
- [139] Michele Vallisneri. Use and abuse of the fisher information matrix in the assessment of gravitational-wave parameter-estimation prospects. *Physical Review D*, 77(4), Feb 2008.
- [140] Eric F. Bell, Daniel H. McIntosh, Neal Katz, and Martin D. Weinberg. The optical and near-infrared properties of galaxies. 1. Luminosity and stellar mass functions. *Astrophys. J. Suppl.*, 149:289, 2003.
- [141] Yen-Ting Lin, Joseph J. Mohr, and S. Adam Stanford. K-band properties of galaxy clusters and groups: Luminosity function, radial distribution and halo occupation number. *Astrophys. J.*, 610:745–761, 2004.
- [142] M. Rahman, S. Nissanke, A. Williamson, et al. 2019. (in preparation).
- [143] Bela Abolfathi et al. The Fourteenth Data Release of the Sloan Digital Sky Survey: First Spectroscopic Data from the Extended Baryon Oscillation Spectroscopic Survey and from the Second Phase of the Apache Point Observatory Galactic Evolution Experiment. *Astrophys. J. Suppl.*, 235(2):42, 2018.
- [144] David J. Schlegel, Douglas P. Finkbeiner, and Marc Davis. Maps of dust IR emission for use in estimation of reddening and CMBR foregrounds. *Astrophys. J.*, 500:525, 1998.
- [145] T. M. C. Abbott et al. The Dark Energy Survey Data Release 2. 1 2021.
- [146] A. Drlica-Wagner et al. Dark Energy Survey Year 1 Results: Photometric Data Set for Cosmology. *Astrophys. J. Suppl.*, 235(2):33, 2018.
- [147] T. M. C. Abbott et al. The Dark Energy Survey Data Release 1. *Astrophys. J. Suppl.*, 239(2):18, 2018.
- [148] Stephane Arnouts, Stefano Cristiani, Lauro Moscardini, Sabino Matarrese, Francesco Lucchin, Adriano Fontana, and Emanuele Giallongo. Measuring and modeling the redshift evolution of clustering: The Hubble Deep Field North. *Mon. Not. Roy. Astron. Soc.*, 310:540–556, 1999.
- [149] Olivier Ilbert et al. Accurate photometric redshifts for the cfht legacy survey calibrated using the vimos vlt deep survey. *Astron. Astrophys.*, 457:841–856, 2006.
- [150] G. Bruzual and Stephane Charlot. Stellar population synthesis at the resolution of 2003. *Mon. Not. Roy. Astron. Soc.*, 344:1000, 2003.
- [151] Gilles Chabrier. Galactic stellar and substellar initial mass function. *Publ. Astron. Soc. Pac.*, 115:763–796, 2003.
- [152] Daniela Calzetti, Anne L. Kinney, and Thaisa Storchi-Bergmann. Dust extinction of the stellar continua in starburst galaxies: The Ultraviolet and optical extinction law. *Astrophys. J.*, 429:582, 1994.

- [153] Claudia Maraston et al. Stellar masses of SDSS-III BOSS galaxies at $z \sim 0.5$ and constraints to galaxy formation models. *Mon. Not. Roy. Astron. Soc.*, 435:2764, 2013.
- [154] Claudia Maraston. Evolutionary population synthesis: Models, analysis of the ingredients and application to high- z galaxies. *Mon. Not. Roy. Astron. Soc.*, 362:799–825, 2005.
- [155] Claudia Maraston, Gustav Stromback, Daniel Thomas, David A. Wake, and Robert C. Nichol. Modeling the color evolution of luminous red galaxies - improvements with empirical stellar spectra. *Mon. Not. Roy. Astron. Soc.*, 394:107, 2009.
- [156] R. Abbott et al. Population Properties of Compact Objects from the Second LIGO-Virgo Gravitational-Wave Transient Catalog. *Astrophys. J. Lett.*, 913(1):L7, 2021.
- [157] Colm Talbot and Eric Thrane. Measuring the binary black hole mass spectrum with an astrophysically motivated parameterization. *Astrophys. J.*, 856(2):173, 2018.
- [158] B. P. Abbott et al. Binary Black Hole Population Properties Inferred from the First and Second Observing Runs of Advanced LIGO and Advanced Virgo. *Astrophys. J. Lett.*, 882(2):L24, 2019.
- [159] Javier Roulet and Matias Zaldarriaga. Constraints on binary black hole populations from LIGO–Virgo detections. *Mon. Not. Roy. Astron. Soc.*, 484(3):4216–4229, 2019.
- [160] Maya Fishbach and Daniel E. Holz. Picky Partners: The Pairing of Component Masses in Binary Black Hole Mergers. *Astrophys. J. Lett.*, 891(1):L27, 2020.
- [161] Alberto Mangiagli, Antoine Klein, Alberto Sesana, Enrico Barausse, and Monica Colpi. Post-Newtonian phase accuracy requirements for stellar black hole binaries with LISA. *Phys. Rev. D*, 99(6):064056, 2019.
- [162] Atsushi Nishizawa, Emanuele Berti, Antoine Klein, and Alberto Sesana. eLISA eccentricity measurements as tracers of binary black hole formation. *Phys. Rev. D*, 94(6):064020, 2016.
- [163] Mark Hannam, Patricia Schmidt, Alejandro Bohé, Leïla Haegel, Sascha Husa, Frank Ohme, Geraint Pratten, and Michael Pürrer. Simple Model of Complete Precessing Black-Hole-Binary Gravitational Waveforms. *Phys. Rev. Lett.*, 113(15):151101, October 2014.
- [164] Zheng-Cheng Liang, Yi-Ming Hu, Yun Jiang, Jun Cheng, Jian-dong Zhang, and Jianwei Mei. Science with the TianQin Observatory: Preliminary Results on Stochastic Gravitational-Wave Background. 7 2021.
- [165] Jian-hua He. Accurate method to determine the systematics due to the peculiar velocities of galaxies in measuring the Hubble constant from gravitational-wave standard sirens. *Phys. Rev. D*, 100(2):023527, 2019.
- [166] Cullan Howlett and Tamara M. Davis. Standard siren speeds: improving velocities in gravitational-wave measurements of H_0 . *Mon. Not. Roy. Astron. Soc.*, 492(3):3803–3815, 2020.
- [167] Constantina Nicolaou, Ofer Lahav, Pablo Lemos, William Hartley, and Jonathan Braden. The Impact of Peculiar Velocities on the Estimation of the Hubble Constant from Gravitational Wave Standard Sirens. *Mon. Not. Roy. Astron. Soc.*, 495(1):90–97, 2020.
- [168] Suvodip Mukherjee, Guilhem Lavaux, François R. Bouchet, Jens Jasche, Benjamin D. Wandelt, Samaya M. Nisanke, Florent Leclercq, and Kenta Hotokezaka. Velocity correction for Hubble constant measurements from standard sirens. *Astron. Astrophys.*, 646:A65, 2021.
- [169] Yan Gong, Xiangkun Liu, Ye Cao, Xuelei Chen, Zuhui Fan, Ran Li, Xiao-Dong Li, Zhigang Li, Xin Zhang, and Hu Zhan. Cosmology from the Chinese Space Station Optical Survey (CSS-OS). *Astrophys. J.*, 883:203, 2019.
- [170] Daniel Foreman-Mackey, David W. Hogg, Dustin Lang, and Jonathan Goodman. emcee: The MCMC Hammer. *Publ. Astron. Soc. Pac.*, 125:306–312, 2013.
- [171] Foreman-Mackey et al. emcee v3: A Python ensemble sampling toolkit for affine-invariant MCMC. *Journal of Open Source Software*, 4:1–2, 2019.
- [172] Ding Qiang Su, Xiangqun Cui, Yanan Wang, and Zhengqiu Yao. Large-sky-area multiobject fiber spectroscopic telescope (LAMOST) and its key technology. In Larry M. Stepp, editor, *Advanced Technology Optical/IR Telescopes VI*, volume 3352 of *Society of Photo-Optical Instrumentation Engineers (SPIE) Conference Series*, pages 76–90, August 1998.
- [173] Xiang-Qun Cui et al. The large sky area multi-object fiber spectroscopic telescope (LAMOST). *Research in Astronomy and Astrophysics*, 12(9):1197–1242, aug 2012.
- [174] Gang Zhao, Yong-Heng Zhao, Yao-Quan Chu, Yi-Peng Jing, and Li-Cai Deng. LAMOST spectral survey — An overview. *Research in Astronomy and Astrophysics*, 12(7):723–734, July 2012.
- [175] Amir Aghamousa et al. The DESI Experiment Part I: Science, Targeting, and Survey Design. 10 2016.
- [176] Roelof S. de Jong et al. 4MOST - 4-metre Multi-Object Spectroscopic Telescope. *Proc. SPIE Int. Soc. Opt. Eng.*, 8446:84460T, 2012.
- [177] Elisabete da Cunha et al. The Taipan Galaxy Survey: Scientific Goals and Observing Strategy. *Publ. Astron. Soc. Austral.*, 34:47, 2017.
- [178] Jonathan P. Gardner et al. The James Webb Space Telescope. *Space Sci. Rev.*, 123:485, 2006.
- [179] Jason Kalirai. Scientific Discovery with the James Webb Space Telescope. *Contemp. Phys.*, 59(3):251–290, 2018.
- [180] J. Green et al. Wide-Field InfraRed Survey Telescope (WFIRST) Final Report. 8 2012.
- [181] R. Chary et al. Joint Survey Processing of Euclid, Rubin and Roman: Final Report. 8 2020.
- [182] Ryan M. O’Leary, Frederic A. Rasio, John M. Fregeau, Natalia Ivanova, and Richard W. O’Shaughnessy. Binary mergers and growth of black holes in dense star clusters. *Astrophys. J.*, 637:937–951, 2006.
- [183] Kyle Kremer, Sourav Chatterjee, Katelyn Breivik, Carl L. Rodriguez, Shane L. Larson, and Frederic A. Rasio. LISA Sources in Milky Way Globular Clusters. *Phys. Rev. Lett.*, 120(19):191103, 2018.
- [184] Leor Barack and Curt Cutler. LISA capture sources: Approximate waveforms, signal-to-noise ratios, and parameter estimation accuracy. *Phys. Rev. D*, 69:082005, 2004.

- [185] Xian Chen and Pau Amaro-Seoane. Revealing the formation of stellar-mass black hole binaries: The need for deci-Hertz gravitational wave observatories. *Astrophys. J. Lett.*, 842(1):L2, 2017.
- [186] Lisa Randall and Zhong-Zhi Xianyu. Eccentricity without Measuring Eccentricity: Discriminating among Stellar Mass Black Hole Binary Formation Channels. *Astrophys. J.*, 914(2):75, 2021.
- [187] V. Gayathri, J. Healy, J. Lange, B. O’Brien, M. Szczepanczyk, I. Bartos, M. Campanelli, S. Klimentko, C. Lousto, and R. O’Shaughnessy. GW190521 as a Highly Eccentric Black Hole Merger. 9 2020.
- [188] V. Gayathri, J. Healy, J. Lange, B. O’Brien, M. Szczepanczyk, I. Bartos, M. Campanelli, S. Klimentko, C. Lousto, and R. O’Shaughnessy. Hubble Constant Measurement with GW190521 as an Eccentric Black Hole Merger. 9 2020.
- [189] Johan Samsing and Daniel J. D’Orazio. Black Hole Mergers From Globular Clusters Observable by LISA I: Eccentric Sources Originating From Relativistic N -body Dynamics. *Mon. Not. Roy. Astron. Soc.*, 481(4):5445–5450, 2018.
- [190] Kevork N. Abazajian et al. The Seventh Data Release of the Sloan Digital Sky Survey. *Astrophys. J. Suppl.*, 182:543–558, 2009.
- [191] Juan De Vicente, Eusebio Sánchez, and Ignacio Sevilla-Noarbe. DNF – Galaxy photometric redshift by Directional Neighbourhood Fitting. *Mon. Not. Roy. Astron. Soc.*, 459(3):3078–3088, 2016.
- [192] V. De Luca, G. Franciolini, P. Pani, and A. Riotto. Primordial Black Holes Confront LIGO/Virgo data: Current situation. *JCAP*, 06:044, 2020.
- [193] Sebastien Clesse and Juan Garcia-Bellido. GW190425, GW190521 and GW190814: Three candidate mergers of primordial black holes from the QCD epoch. 7 2020.
- [194] V. De Luca, V. Desjacques, G. Franciolini, P. Pani, and A. Riotto. GW190521 Mass Gap Event and the Primordial Black Hole Scenario. *Phys. Rev. Lett.*, 126(5):051101, 2021.
- [195] V. De Luca, G. Franciolini, P. Pani, and A. Riotto. Bayesian Evidence for Both Astrophysical and Primordial Black Holes: Mapping the GWTC-2 Catalog to Third-Generation Detectors. *JCAP*, 05:003, 2021.
- [196] Heling Deng. A possible mass distribution of primordial black holes implied by LIGO-Virgo. *JCAP*, 04:058, 2021.
- [197] Matt Visser. Jerk, snap and the cosmological equation of state. *Class. Quant. Grav.*, 21:2603–2616, 2004.
- [198] Yun-Gui Gong. Model independent analysis of dark energy. 1. Supernova fitting result. *Class. Quant. Grav.*, 22:2121–2133, 2005.
- [199] En-Kun Li, Minghui Du, Zhi-Huan Zhou, Hongchao Zhang, and Lixin Xu. Testing the effect of H_0 on $f\sigma_8$ tension using a Gaussian process method. *Mon. Not. Roy. Astron. Soc.*, 501(3):4452–4463, 2021.
- [200] Imre Bartos, Arlin P. S. Crofts, and Szabolcs Márka. Galaxy Survey On The Fly: Prospects of Rapid Galaxy Cataloging to Aid the Electromagnetic Follow-up of Gravitational-wave Observations. *Astrophys. J. Lett.*, 801(1):L1, 2015.
- [201] Hsin-Yu Chen and Daniel E. Holz. Facilitating follow-up of LIGO-Virgo events using rapid sky localization. *Astrophys. J.*, 840:88, 2017.
- [202] N. J. Klingler et al. *Swift*-XRT Follow-up of Gravitational Wave Triggers in the Second Advanced LIGO/Virgo Observing Run. *Astrophys. J. Suppl.*, 245(1):15, 2019.
- [203] T. Abbott et al. The dark energy survey. 10 2005.
- [204] I. Sevilla-Noarbe et al. Dark Energy Survey Year 3 Results: Photometric Data Set for Cosmology. 11 2020.
- [205] Chunyu Zhang, Qing Gao, Yungui Gong, Dicong Liang, Alan J. Weinstein, and Chao Zhang. Frequency response of time-delay interferometry for space-based gravitational wave antenna. *Phys. Rev. D*, 100(6):064033, 2019.
- [206] Alexandre Toubiana, Sylvain Marsat, Stanislav Babak, John Baker, and Tito Dal Canton. Parameter estimation of stellar-mass black hole binaries with LISA. *Phys. Rev. D*, 102:124037, 2020.
- [207] S. Karki et al. The Advanced LIGO Photon Calibrators. *Rev. Sci. Instrum.*, 87(11):114503, 2016.
- [208] Ling Sun et al. Characterization of systematic error in Advanced LIGO calibration. *Class. Quant. Grav.*, 37(22):225008, 2020.
- [209] D. Estevez, P. Lagabbe, A. Masserot, L. Rolland, M. Seglar-Arroyo, and D. Verkindt. The Advanced Virgo Photon Calibrators. *Class. Quant. Grav.*, 38(7):075007, 2021.
- [210] Stéfan van der Walt, S. Chris Colbert, and Gaël Varoquaux. The NumPy Array: A Structure for Efficient Numerical Computation. *Comput. Sci. Eng.*, 13(2):22–30, 2011.
- [211] Pauli Virtanen et al. SciPy 1.0–Fundamental Algorithms for Scientific Computing in Python. *Nature Meth.*, 17:261, 2020.
- [212] LIGO Scientific Collaboration. LIGO Algorithm Library - LALSuite. free software (GPL), 2018.
- [213] John D. Hunter. Matplotlib: A 2D Graphics Environment. *Comput. Sci. Eng.*, 9(3):90–95, 2007.
- [214] Daniel Foreman-Mackey. corner.py: Scatterplot matrices in python. *The Journal of Open Source Software*, 1(2):24, jun 2016.